Journal Name

COMMUNICATION

An Iminodibenzyl-Quinoxaline-Iminodibenzyl Scaffold as a Mechanochromic and Dual Emitter: Donor and Bridge Effects on Optical Properties

Received 00th January 20xx,
Accepted 00th January 20xx

DOI: 10.1039/x0xx00000x

www.rsc.org/

Ramin Pashazadeh,[a] Piotr Pander,[b] Audrius Bucinskas,[a] Peter J. Skabara,[c] Fernando B. Dias,*[b] Juozas V. Grazulevicius*[a]

The influence of phenyl linkage and donor strength on the photophysical properties of new derivatives of quinoxaline-containing iminodibenzyl and iminostilbene moieties is studied. The donor-acceptor derivatives showed dual thermally activated delayed fluorescence (TADF) and room temperature phosphorescence (RTP) despite a large energy gap between the excited singlet and triplet states (ca. 0.5 eV). This extremely rare observation is explained by the twisted and rigidified structure of the iminodibenzyl moiety.

Luminogens that demonstrate room temperature phosphorescence (RTP) have attracted great interest due to their long-lived triplet excitons and their potential application in various fields, such as biological imaging, data encryption and luminescent sensors.[1] RTP materials typically contain noble metals to promote intersystem crossing between the excited singlet and triplet state through the influence of increased spin-orbit coupling (SOC).[2] Strategies to enhance RTP have been devoted to the restriction of molecular vibration and rotation, isolation from triplet quenchers such as oxygen and moisture and doping in a rigid matrix.[3] However, due to the large cost, scarcity and toxicity of noble metals, scientists have been motivated to explore alternative purely organic phosphors, advantageous through their versatile molecular design and low cost.[4]

Metal-free purely organic thermally activated delayed fluorescence (TADF) materials, which are able to realise 100% internal quantum efficiency of organic light emitting diodes (OLEDs), have attracted great interest.[5] Spin statistics in OLEDs leads to the formation of dark 75% triplet states, and 25% emissive singlet states upon charge carrier recombination. Therefore, the internal quantum efficiency (IQE) of OLEDs using standard fluorescent emitters is limited to 25%. Through decreasing energy splitting between singlet and triplet states (ΔE_{ST}), typically below 0.3 eV, electrons in the triplet state are able to up-convert into the singlet state by reverse intersystem crossing (RISC) to generate singlet excitons.[5,6]

In general, a luminogen scaffold is comprised of donor and acceptor moieties. Although many new acceptors have been introduced, research on new donors is less developed with carbazole, diphenylamine, phenothiazine, 9,9-dimethyl-acridine, and phenoxazine are the major building blocks used on the design of most TADFs.[7] In general, chemists tend to add substituents on the known donors, thus modifying their properties. Iminodibenzyl (IDB) and iminostilbene (ISB) used in this work are commercially available low-cost electron rich compounds. Although these moieties are well-known,[8] little attention has been given to their performance in donor-acceptor-donor (D-A-D) luminogens. Iminodibenzyl (**Fig 1**) contains a twisted 7-membered ring structure to which two benzene rings are fused. Its construction is similar to that of diphenylamine, but contains an ethylene bridge which suppresses molecular twisting, i.e. rotation of the phenyl rings along the C-N axis. On the contrary, iminostilbene is a 7-membered anti-aromatic structure.[9] In 2008, Ho *et al.* reported the application of iminodibenzyl in the preparation of a blue OLED device.[10] Recently, Huang and co-workers introduced iminodibenzyl as an organic phosphorescent emitter with ultra long emission lifetime of 402 ms under ambient conditions.[11]

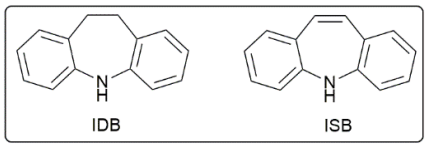

Fig 1. Molecular structure of iminodibenzyl (IDB) and iminostilbene (ISB)

To date, only a few reports of dual emission with room temperature fluorescence-phosphorescence properties have been published.[12] In 2017 Dias *et al.* and in 2018 Ray *et al*. introduced dual emission (TADF and RTP) and probed the thermal effects on the intensity of emission.[13] To observe room temperature TADF-phosphorescence, a larger singlet-triplet splitting is necessary to slow down the RISC rate in order to harvest triplet excitons directly (phosphorescence), but not too large to stop RISC completely. We recently

[a] *Department of Polymer Chemistry and Technology, Kaunas University of Technology, Kaunas, Lithuania.*
[b] *Department of Physics, University of Durham, South Road DH1 3LE, Durham, UK.*
[c] *WestCHEM, School of Chemistry, University of Glasgow, Glasgow G12 8QQ, UK*
† *Emails: juozas.grazulevicius@ktu.lt, f.m.b.dias@durham.ac.uk.*
Electronic Supplementary Information (ESI) available: Details of synthetic procedures, photophysical, thermal, electrochemical properties and single crystal data (PDF). See DOI: 10.1039/x0xx00000x

demonstrated quinoxaline as a promising acceptor to prepare multifunctional TADF materials.[14] Herein, we report on the design and synthesis of new luminogens based on quinoxaline as the electron acceptor and IDB/ISB as electron donors (**Fig 2**). We initially studied the photophysical behaviour of AzQx, and demonstrated the dual RTP-TADF luminescence of this compound in Zeonex. A phenylene group was introduced between the donor and acceptor moieties, working as a bridge in compounds IDBQx, ISBQx and OIDBQx. IDBQx showed dual emission, consisting of blue TADF and orange RTP emission. These results indicate that the twisted and non-aromatic conformation of IDB suppresses the non-radiative decay, but also induces strong spin-orbit coupling, so that both TADF and phosphorescence can be observed clearly at room temperature. Noteworthy, no delayed fluorescence or RTP were observed for ISBQx, which exhibited only prompt fluorescence. The boat shape structure of the 7-membered ring of ISB in ISBQx is thereby supports non-radiative processes, which in turn quench triplet excitons. Thus, at room temperature, ISBQx showed solely prompt fluorescence.

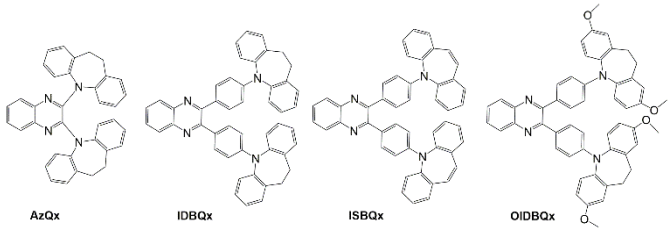

Fig 2. Chemical structures of the compounds investigated in this study

The synthetic routes and experimental data for the target compounds are described in in the supporting information. AzQx was prepared from the reaction of 2,3-dicholoroquinoxaline and IDB in the presence of $ZnCl_2$. The syntheses of the luminogens with the phenylene bridges was conducted in two steps. Firstly, reaction of *o*-phenylenediamine with 4,4'-dibromobenzil in the presence of HCl and AcOH, gave the dibromo derivative of the extended quinoxaline acceptor. *N*-Arylation of the dibromo derivative through Buchwald-Hartwig reaction with IDB or ISB yielded the target products.[15] The structures of the compounds were confirmed with ^{1}H NMR, ^{13}C NMR and mass spectrometry.

The thermal analysis of compounds showed that compounds with phenylene linkage present higher stabilities, indicating stronger intermolecular interactions (**Fig. S6 and S7**). The single crystal XRD analysis (**Fig. 3**) of IDBQx and ISBQx revealed their molecular conformations. To minimise steric hindrance between the donor and phenyl linkage, the 7-membered ring core of the donor is distorted giving a bent conformation. IDBQx demonstrated a twist-boat form, while a boat conformation was observed for ISBQx. Because of these adopted conformations the donor-acceptor dihedral angles were found to be relatively small, at *ca*. 11° and 12° for IDBQx and ISBQx, respectively.

The studied molecules, due to their bipolar, donor-acceptor structure showed pronounced solvatochromism (**Fig. 4**). For the molecules containing the phenylene spacer (IDBQx, ISBQx and OIDBQx), the CT character was found to be less expressed than for AzQx, which contains no π-spacer. The emission colour of IDBQx, ISBQx and OIDBQx varied from blue for solutions in cyclohexane to green for solutions in highly polar acetonitrile.

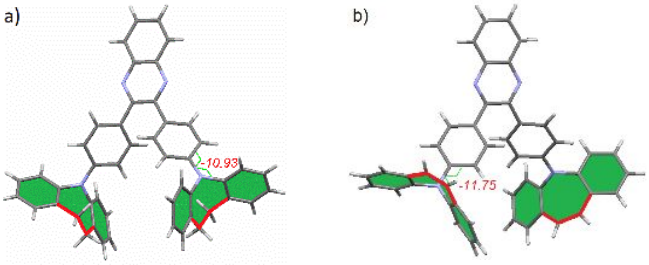

Fig 3: Single crystal structures of a) IDBQx and b) ISBQx. Dihedral angles between donor and phenyl ring are depicted.

In contrast to the other molecules, AzQx showes blue emission in cyclohexane and orange-red emission in acetonitrile. In AzQx the lack of a spacer forces the spacious iminodibenzyl groups to adopt a more twisted conformation in quasi-orthogonal D-A orientation, thus the CT singlet excited state is further stabilized. The absorption band at *ca*. 400 nm in the spectra of all the molecules is attributed to a CT-ππ* transition as indicated by its positive solvatochromism.

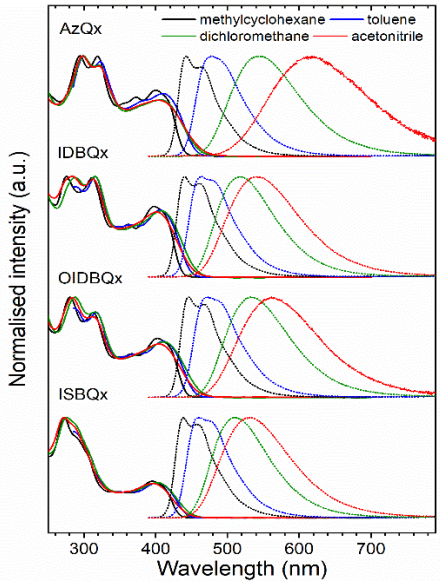

Fig 4. Absorption and photoluminescence spectra of the solutions in various solvents.

Although the molecules did not show delayed fluorescence in solutions, they showed an interesting behaviour in Zeonex solid films (**Fig. 5**). Due to the non-polarity of Zeonex, fluorescence of iminodibenzyl and iminostilbene derivatives were similar to cyclohexane or toluene solutions (i.e. in the blue region). This implies a large singlet-triplet gap of ≈0.5 eV (**Table 1**), thus preventing efficient thermally activated reverse intersystem crossing. For this reason, the molecules did not show significant contributions of TADF at room temperature. However, unexpectedly, molecules with IDB showed strong room temperature phosphorescence. In fact, only the iminodibenzyl derivatives demonstrated delayed emission at room temperature, while the iminostilbene derivative was found to be a purely fluorescent system. This observation might be explained by the

Table 1. Photophysical characteristics.

Sample	Abs (nm)[a]	PL (nm)[b]	Φ_{PL}[c]	S_1 / T_1 (eV)[d]	ΔE_{ST} (eV)[e]	$T_c/T_g/T_d$[f] (°C)	HOMO/LUMO (eV)[g]	E_g (eV)[h]
AzQx	299, 321, 406	545	0.41	2.92 / 2.41	0.51	-/110/242	-5.23/-2.77	2.68
IDBQx	288, 315, 408	518	0.38	2.93 / 2.41	0.52	182/145/402	-5.39/-2.79	2.71
OIDBQx	287, 315, 411	534	0.31	2.88 / 2.39	0.49	198/146/398	-5.26/-2.75	2.68
ISBQx	276, 402	511	0.35	2.91 / 2.40	0.51	284/165/418	-5.41/-2.76	2.75

[a]absorption maxima in CH_2Cl_2 solution; [b]emission maxima in CH_2Cl_2 solution; [c]PL quantum yield in degassed CH_2Cl_2 solution; [d]singlet and triplet energy in Zeonex 1% (w/w) film; [e]singlet-triplet energy splitting in Zeonex 1% (w/w) film; [f]crystallisation (T_c), glass transition (T_g) and decomposition (T_d) temperatures determined by DSC and TGA measurements; [g]determined by cyclic voltammetry in CH_2Cl_2; [h]optical energy gap in CH_2Cl_2.

suppression of non-radiative decay playing an important role in enabling the long-lived emissions.

Although the iminostilbene intuitively appears more rigid than iminostilbene, the authors speculate that in fact the iminostilbene is relatively free to interconvert between chiral conformations, thus giving a fluttering motion. However, the singlet-triplet energy gap is still sufficient to allow thermal energy to partially up-convert the triplet states, and this is the reason why simultaneous TADF and RTP emissions were observed for derivatives of the iminodibenzyl compounds.

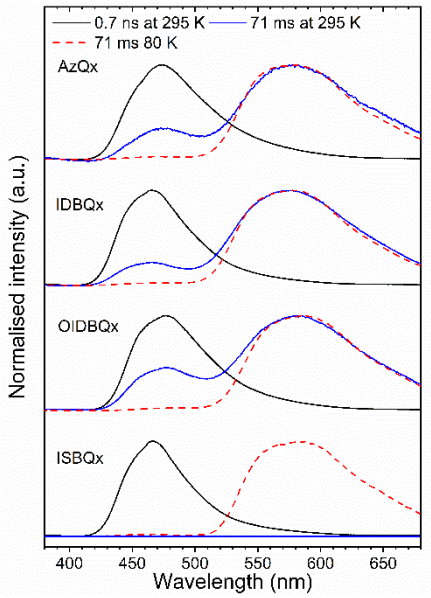

Fig 5. Prompt fluorescence (black solid line), room temperature phosphorescence and TADF (blue solid line), low temperature phosphorescence (red dashed line) spectra of molecular dispersions of the compounds in Zeonex.

The existence of TADF and absence of triplet-triplet annihilation was evidenced by the linear dependence of the intensity of the delayed fluorescence emission with laser dose, e.g. the slope of DF intensity vs. excitation power is equal 1 in log-log scale (see **Fig 6a** and **Fig 6c** and **Fig S13, S14** in the SI).[14] In general, the ratio between TADF and RTP correlates with the $\Delta E_{S\text{-}T}$, and in this respect the largest contribution of TADF was observed for OIDBQx. The ratio of intensities of RTP and TADF does not change with delay time for OIDBQx, which is also evidenced by monoexponential decay. This observation shows that both emissions originate from the same excited triplet state and both arrive from the same population of excited states. TADF+RTP dual emission of the derivatives of iminodibenzyl is strong and easily noticeable as a yellow-greenish afterglow. Furthermore, the lifetime of the TADF+RTP emission is relatively long, spanning from 51 ± 3 ms for AzQx to a remarkable 128 ± 10 ms for OIDBQx (see **Fig S9-S11** in the SI).

Such a behaviour can be explained by the suppression of the non-radiative decay of the triplet state and by substantial triplet formation yields. The non-bonding orbitals, such as those present in the donor unit, predetermine high triplet formation yields, due to the creation of n-π* transitions, which induce strong spin-orbit coupling, according to El-Sayed's rule. Both non-radiative decay and RISC process affect the iminodibenzyl derivatives, which is evidenced by substantially longer phosphorescence lifetimes observed at 80 K compared to the lifetime of TADF+RTP emissions recorded at 295 K. Remarkably, this is not the case in OIDBQx, where the two emissions show lifetimes that are statistically insignificantly different at different temperature (see **Fig S11** in the SI). The methoxy substitution not only stabilises the triplet state but appears to induce the largest triplet formation yield; in turn the TADF+RTP emission is the most efficient for OIDBQx. This can be caused either by inducing a larger contribution of the non-bonding pairs to the excited state by the introduction of the methoxy groups or by the fact that the $\Delta E_{S\text{-}T}$ is the smallest (which improves the coupling of the S_1 and T_1 states).

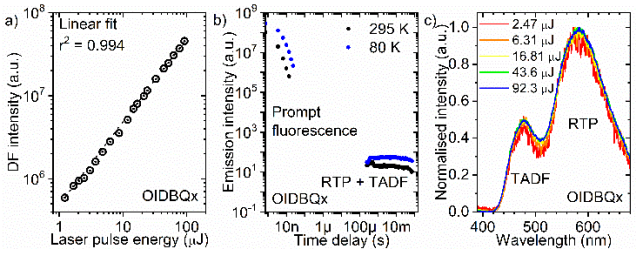

Fig 6. a) Power dependence of delayed fluorescence of OIDBQx at 295 K; b) photoluminescence decay transients of OIDBQx at 295 and 80 K; c) delayed fluorescence and room temperature phosphorescence spectra recorded at 295 K with various excitation pulse energy.

In mechanochromic materials increasing the strength of acceptor leads to stronger mechanochromism.[16] Interestingly, OIDBQx displays reversible luminescence changes upon applying external stress (**Fig 7**). The initial powder demonstrated greenish-blue emission with λ_{max} = 494 nm. Through grinding the initial powder with a spatula the emission broadened and red-shifted to 522 nm. The initial state was restored by exposure to CH_2Cl_2 vapour for 5 min. The vapour-treated form produced an emission spectrum nearly identical to that of the initial powder (λ_{max} = 495 nm). Neat film showed a similar emission spectrum to that of the ground powder. In comparison with powder XRD data, initial and fumed forms appeared to be crystalline, whereas ground and neat film were amorphous (**Fig S16**). Additionally, in ground form and neat

film the prompt fluorescence lifetimes were longer than in the initial and fumed forms (**Table 1 SI**). This implies stronger charge transfer character of the singlet excited state in the amorphous forms. In contrast, insignificant changes were observed in the emission of IDBQx under grinding. The photoluminescence maximum shifted from 495 nm to 499 nm. These results indicate that increasing the strength of the electron donor by methoxylation of IDB can increase colour contrast upon the application of external stimuli, in agreement with previous work.[14]

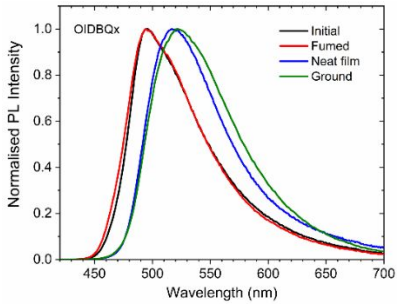

Fig 7. PL spectra of OIDBQx in different forms. Neat film obtained by drop casting.

In summary, we have designed and synthesised four new derivatives of quinoxaline-containing iminodibenzyl and iminostilbene moieties and studied their photophysical properties. These luminophores showed room temperature delayed fluorescence and phosphorescence, despite having a large singlet-triplet energy gap. An increase of the dipole moment of the iminodibenzyl derivative containing methoxy groups caused mechanochromic luminescent behaviour. The lifetime of room-temperature phosphorescence was found to increase through the introduction of a phenyl spacer between the donor and acceptor moieties and further increased by substitution of the iminodibenzyl moiety with methoxy groups. The investigations revealed that a twisted iminodibenzyl is a promising donor to suppress non-radiative decay.

Conflicts of interest

There are no conflicts to declare.

Acknowledgments

This work was supported by the project EXCILIGHT, funded by the European Union's Horizon 2020 Research and Innovation Programme under grant agreement no. 674990. We thanks Dr Nils Trapp (Dep. of Chemistry and Applied Biosc., ETH Zürich) for the help of single crystal XRD analysis. We also thank Dr Algirdas Lazauskas (Inst. of Materials Science, Kaunas University of Technology) for assistance with PXRD measurements.

Notes and references

1- (a) P. Lehner, C. Staudinger, S. M. Borisov and I. Klimant, *Nat. Commun.*, 2014, **5**, 4460. (b) R. I. Dmitriev, A. V. Kondrashina, K. Koren, I. Klimant, A. V. Zhdanov, J. M. P. Pakan, K. W. McDermott and D. B. Papkovsky, *Biomater. Sci.*, 2014, **2**, 853–866. (c) Y. Deng, D. Zhao, X. Chen, F. Wang, H. Song and D. Shen, *Chem. Commun.*, 2013, **49**, 5751–5753.

2- M. Quaranta, S. M. Borisov and I. Klimant, *Bioanal. Rev.,* 2012, **4**, 115– 157.

3- (a) D. Lee, O. Bolton, B. C. Kim, J. H. Youk , S. Takayama and J. Kim, *J. Am. Chem. Soc.*, 2013, **135**, 6325. (b) D. Li, F. Lu, J. Wang, W. Hu, X.-M. Cao, X. Ma and H. Tian, *J. Am. Chem. Soc.*, 2018, **140**, 1916.

4- (a) Y. Shoji, Y. Ikabata, Q. Wang, D. Nemoto, A. Sakamoto, N. Tanaka, J. Seino, H. Nakai and T. Fukushima, *J. Am. Chem. Soc.,* 2017, **139**, 2728 (b) P. Pander, A. Swist, R. Motyka, J. Soloducho, F. B. Dias and P. Data, *J. Mater. Chem. C,* 2018*,* **6***,* 5434-5443*.* (c) X. Ma, C. Xu, J. Wang and H. Tian, *Angew. Chem. Int. Ed.,* 2018, **57**, 1.

5- (a) Z. Yang, Z. Mao, Z. Xie, Y. Zhang, S. Liu, J. Zhao, J. Xu, Z. Chi and M. P. Aldred, *Chem. Soc. Rev.*, 2017, **46**, 915. (b) G. Grybauskaite-Kaminskiene, K. Ivaniuk, G. Bagdziunas, P. Turyk, P. Stakhira, G. Baryshnikov, D. Volyniuk, V. Cherpak, B. Minaev, Z. Hotra, H. Agren and J. V. Grazulevicius, *J. Mater. Chem. C*, 2018, **6**, 1543-1550. (c) T. Matulaitis, P. Imbrasas, N. A. Kukhta, P. Baronas, T. Buciunas, D. Banevicius, K. Kazlauskas, J. V. Grazulevicius and S. Jursenas, *J. Phys. Chem. C*, 2017, **121**, 23618–23625.

6- (a) C. Li, Y. Wang, D. Sun, H. Li, X. Sun, D. Ma, Z. Ren and S. Yan, *ACS Appl. Mater. Interfaces*, 2018, **10**, 5731. (b) S. Shao, J. Hu, X. Wang, L. Wang, X. Jing and F. Wang, *J. Am. Chem. Soc.*, 2017, **139**, 17739.

7- (a) M. Y. Wong and E. Zysman-Colman, *Adv. Mater.,* 2017, 1605444. (b) P. Schrogel, A. Tomkevicienė, P. Strohriegl, S. T. Hoffmann, A. Kohlerb and C. Lennartz, *J. Mater. Chem.*, 2011, **21**, 2266-2273.

8- (a) Z. Wang and W. G. McGimpsey, *J. Phys. Chem.*, 1993, **97**, 9668–9672. (b) S. Dollinger, S. Löber, R. Klingenstein, C. Korth and P. Gmeiner, *J. Med. Chem.*, 2006, **49**, 6591 (c) L. J. Kricka and A. Ledwith, *Chem. Rev.*, 1974, **74**, 101.

9- C. Dardonville, M. L. Jimeno, I. Alkorta and J. Elguero, *Org. Biomol. Chem.*, 2004, **2**, 1587-1591.

10- M.-H. Ho, C.-M. Chang, T.-Y. Chu, T.-M. Chen and C. H. Chen, *Org. Electron.*, 2008, **9**, 101–110.

11- C. Sun, X. Ran, X. Wang, Z. Cheng, Q. Wu, S. Cai, L. Gu, N. Gan, H. Shi, Z. An, H. Shi and W. Huang, *J. Phys. Chem. Lett.*, 2018, **9**, 335.

12- (a) Z. Mao, Z. Yang, Y. Mu, Y. Zhang, Y. F. Wang, Z. Chi, C. C. Lo, S. Liu, A. Lien and J. Xu, *Angew. Chem. Int. Ed.,* 2015, **54**, 6270–6273. (b) L. Xiao, Y. Wu, J. Chen, Z. Yu, Y. Liu, J. Yao and H. Fu, *J. Phys. Chem. A*, 2017, **121**, 8652 (c) D. Li, F. Lu, J. Wang, W. Hu, X.-M. Cao, X. Ma and H. Tian, *J. Am. Chem. Soc.*, 2018, **140**, 1916.

13- (a) R. Huang, J. Avo, T. Northey, E. Chaning-Pearce, P. L. D. Santos, J. S. Ward, P. Data, M. K. Etherington, M. A. Fox, T. J. Penfold, M. N. Berberan-Santos, J. C. Lima, M. R. Bryce and F. B. Dias, *J. Mater. Chem. C*, 2017, **5**, 6269. (b) I. Bhattacharjee, N. Acharya, H. Bhatia and D. Ray, *J. Phys. Chem. Lett.*, 2018, **9**, 2733. (c) Y. Takeda, T. Kaihara, M. Okazaki, H. Higginbotham, P. Data, N. Tohnai and S. Minakata, *Chem. Commun.*, 2018, **54**, 6847–6850.

14- R. Pashazadeh, P. Pander, A. Lazauskas, F. B. Dias and J. V. Grazulevicius, *J. Phys. Chem. Lett.*, 2018, **9**, 1172–1177.

15- (a) O. Vybornyi, N. J. Findlay and P. J. Skabara, *J. Vis. Exp.*, 2017, (128), e56501. (b) W. Huang and S. L. Buchwald, *Chem.–Eur. J.*, 2016, **22**, 14186–14189.

16- T. Jadhav, B. Dhokale and R. Misra, *J. Mater. Chem. C*, 2015, **3**, 9063-9068.

Graphical abstract

Dual emission (TADF+RTP) and mechanochromism have been obtained using an iminodibenzyl-quinoxaline-iminodibenzyl scaffold.

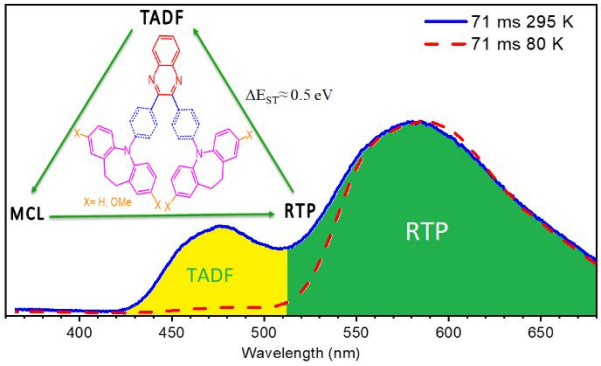

Journal Name

COMMUNICATION

An Iminodibenzyl-Quinoxaline-Iminodibenzyl Scaffold as a Mechanochromic and Dual Emitter: Donor and Bridge Effects on Optical Properties

Received 00th January 20xx,
Accepted 00th January 20xx

DOI: 10.1039/x0xx00000x

www.rsc.org/

Ramin Pashazadeh,[a] Piotr Pander,[b] Audrius Bucinskas,[a] Peter J. Skabara,[c] Fernando B. Dias,*[b] Juozas V. Grazulevicius*[a]

The influence of phenyl linkage and donor strength on the photophysical properties of new derivatives of quinoxaline-containing iminodibenzyl and iminostilbene moieties is studied. The donor-acceptor derivatives showed dual thermally activated delayed fluorescence (TADF) and room temperature phosphorescence (RTP) despite a large energy gap between the excited singlet and triplet states (ca. 0.5 eV). This extremely rare observation is explained by the twisted and rigidified structure of the iminodibenzyl moiety.

Luminogens that demonstrate room temperature phosphorescence (RTP) have attracted great interest due to their long-lived triplet excitons and their potential application in various fields, such as biological imaging, data encryption and luminescent sensors.[1] RTP materials typically contain noble metals to promote intersystem crossing between the excited singlet and triplet state through the influence of increased spin-orbit coupling (SOC).[2] Strategies to enhance RTP have been devoted to the restriction of molecular vibration and rotation, isolation from triplet quenchers such as oxygen and moisture and doping in a rigid matrix.[3] However, due to the large cost, scarcity and toxicity of noble metals, scientists have been motivated to explore alternative purely organic phosphors, advantageous through their versatile molecular design and low cost.[4]

Metal-free purely organic thermally activated delayed fluorescence (TADF) materials, which are able to realise 100% internal quantum efficiency of organic light emitting diodes (OLEDs), have attracted great interest.[5] Spin statistics in OLEDs leads to the formation of dark 75% triplet states, and 25% emissive singlet states upon charge carrier recombination. Therefore, the internal quantum efficiency (IQE) of OLEDs using standard fluorescent emitters is limited to 25%. Through decreasing energy splitting between singlet and triplet states (ΔE_{ST}), typically below 0.3 eV, electrons in the triplet state are able to up-convert into the singlet state by reverse intersystem crossing (RISC) to generate singlet excitons.[5,6]

In general, a luminogen scaffold is comprised of donor and acceptor moieties. Although many new acceptors have been introduced, research on new donors is less developed with carbazole, diphenylamine, phenothiazine, 9,9-dimethyl-acridine, and phenoxazine are the major building blocks used on the design of most TADFs.[7] In general, chemists tend to add substituents on the known donors, thus modifying their properties. Iminodibenzyl (IDB) and iminostilbene (ISB) used in this work are commercially available low-cost electron rich compounds. Although these moieties are well-known,[8] little attention has been given to their performance in donor-acceptor-donor (D-A-D) luminogens. Iminodibenzyl (**Fig 1**) contains a twisted 7-membered ring structure to which two benzene rings are fused. Its construction is similar to that of diphenylamine, but contains an ethylene bridge which suppresses molecular twisting, i.e. rotation of the phenyl rings along the C-N axis. On the contrary, iminostilbene is a 7-membered anti-aromatic structure.[9] In 2008, Ho *et al.* reported the application of iminodibenzyl in the preparation of a blue OLED device.[10] Recently, Huang and co-workers introduced iminodibenzyl as an organic phosphorescent emitter with ultra long emission lifetime of 402 ms under ambient conditions.[11]

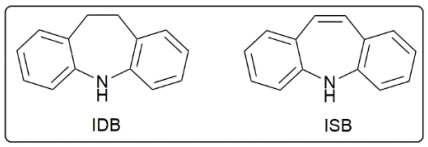

Fig 1. Molecular structure of iminodibenzyl (IDB) and iminostilbene (ISB)

To date, only a few reports of dual emission with room temperature fluorescence-phosphorescence properties have been published.[12] In 2017 Dias *et al.* and in 2018 Ray *et al*. introduced dual emission (TADF and RTP) and probed the thermal effects on the intensity of emission.[13] To observe room temperature TADF-phosphorescence, a larger singlet-triplet splitting is necessary to slow down the RISC rate in order to harvest triplet excitons directly (phosphorescence), but not too large to stop RISC completely. We recently

[a] *Department of Polymer Chemistry and Technology, Kaunas University of Technology, Kaunas, Lithuania.*
[b] *Department of Physics, University of Durham, South Road DH1 3LE, Durham, UK.*
[c] *WestCHEM, School of Chemistry, University of Glasgow, Glasgow G12 8QQ, UK*
† *Emails: juozas.grazulevicius@ktu.lt, f.m.b.dias@durham.ac.uk.*
Electronic Supplementary Information (ESI) available: Details of synthetic procedures, photophysical, thermal, electrochemical properties and single crystal data (PDF). See DOI: 10.1039/x0xx00000x

demonstrated quinoxaline as a promising acceptor to prepare multifunctional TADF materials.[14] Herein, we report on the design and synthesis of new luminogens based on quinoxaline as the electron acceptor and IDB/ISB as electron donors (**Fig 2**). We initially studied the photophysical behaviour of AzQx, and demonstrated the dual RTP-TADF luminescence of this compound in Zeonex. A phenylene group was introduced between the donor and acceptor moieties, working as a bridge in compounds IDBQx, ISBQx and OIDBQx. IDBQx showed dual emission, consisting of blue TADF and orange RTP emission. These results indicate that the twisted and non-aromatic conformation of IDB suppresses the non-radiative decay, but also induces strong spin-orbit coupling, so that both TADF and phosphorescence can be observed clearly at room temperature. Noteworthy, no delayed fluorescence or RTP were observed for ISBQx, which exhibited only prompt fluorescence. The boat shape structure of the 7-membered ring of ISB in ISBQx is thereby supports non-radiative processes, which in turn quench triplet excitons. Thus, at room temperature, ISBQx showed solely prompt fluorescence.

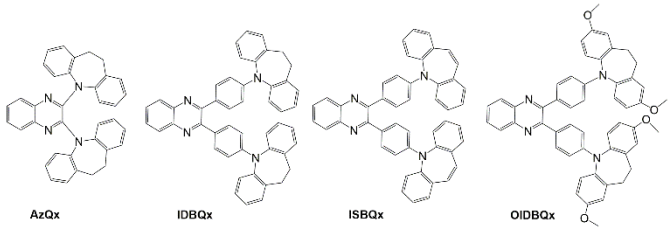

Fig 2. Chemical structures of the compounds investigated in this study

The synthetic routes and experimental data for the target compounds are described in in the supporting information. AzQx was prepared from the reaction of 2,3-dicholoroquinoxaline and IDB in the presence of $ZnCl_2$. The syntheses of the luminogens with the phenylene bridges was conducted in two steps. Firstly, reaction of *o*-phenylenediamine with 4,4'-dibromobenzil in the presence of HCl and AcOH, gave the dibromo derivative of the extended quinoxaline acceptor. *N*-Arylation of the dibromo derivative through Buchwald-Hartwig reaction with IDB or ISB yielded the target products.[15] The structures of the compounds were confirmed with ^{1}H NMR, ^{13}C NMR and mass spectrometry.

The thermal analysis of compounds showed that compounds with phenylene linkage present higher stabilities, indicating stronger intermolecular interactions (**Fig. S6 and S7**). The single crystal XRD analysis (**Fig. 3**) of IDBQx and ISBQx revealed their molecular conformations. To minimise steric hindrance between the donor and phenyl linkage, the 7-membered ring core of the donor is distorted giving a bent conformation. IDBQx demonstrated a twist-boat form, while a boat conformation was observed for ISBQx. Because of these adopted conformations the donor-acceptor dihedral angles were found to be relatively small, at *ca*. 11° and 12° for IDBQx and ISBQx, respectively.

The studied molecules, due to their bipolar, donor-acceptor structure showed pronounced solvatochromism (**Fig. 4**). For the molecules containing the phenylene spacer (IDBQx, ISBQx and OIDBQx), the CT character was found to be less expressed than for AzQx, which contains no π-spacer. The emission colour of IDBQx, ISBQx and OIDBQx varied from blue for solutions in cyclohexane to green for solutions in highly polar acetonitrile.

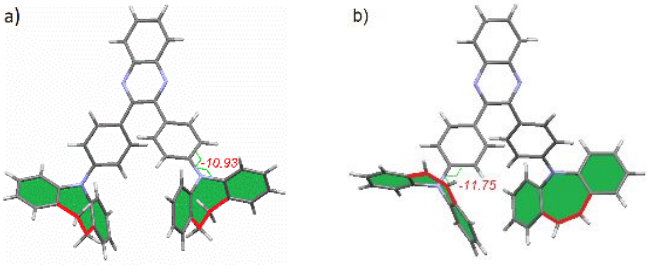

Fig 3: Single crystal structures of a) IDBQx and b) ISBQx. Dihedral angles between donor and phenyl ring are depicted.

In contrast to the other molecules, AzQx showes blue emission in cyclohexane and orange-red emission in acetonitrile. In AzQx the lack of a spacer forces the spacious iminodibenzyl groups to adopt a more twisted conformation in quasi-orthogonal D-A orientation, thus the CT singlet excited state is further stabilized. The absorption band at *ca*. 400 nm in the spectra of all the molecules is attributed to a CT-ππ* transition as indicated by its positive solvatochromism.

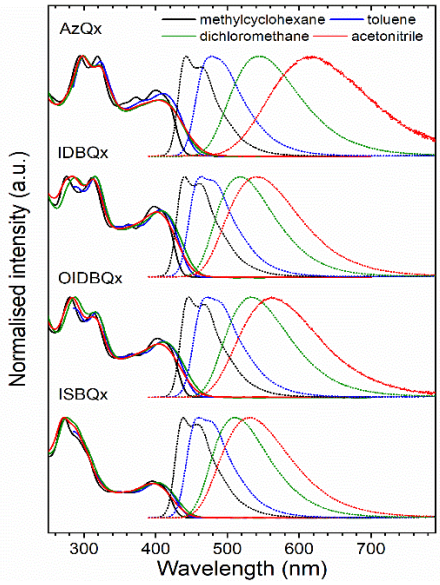

Fig 4. Absorption and photoluminescence spectra of the solutions in various solvents.

Although the molecules did not show delayed fluorescence in solutions, they showed an interesting behaviour in Zeonex solid films (**Fig. 5**). Due to the non-polarity of Zeonex, fluorescence of iminodibenzyl and iminostilbene derivatives were similar ~~to observed for~~ cyclohexane or toluene solutions (i.e. in the blue region). This implies a large singlet-triplet gap of ≈0.5 eV (**Table 1**), thus preventing efficient thermally activated reverse intersystem crossing. For this reason, the molecules did not show significant contributions of TADF at room temperature. However, unexpectedly, molecules with IDB showed strong room temperature phosphorescence. In fact, only the iminodibenzyl derivatives demonstrated delayed emission at room temperature, while the iminostilbene derivative was found to be a purely fluorescent system. This observation might be explained by the

Table 1. Photophysical characteristics.

Sample	Abs (nm)[a]	PL (nm)[b]	Φ_{PL}[c]	S_1 / T_1 (eV)[d]	ΔE_{ST} (eV)[e]	$T_c/T_g/T_d$[f] (°C)	HOMO/LUMO (eV)[g]	E_g (eV)[h]
AzQx	299, 321, 406	545	0.41	2.92 / 2.41	0.51	-/110/242	-5.23/-2.77	2.68
IDBQx	288, 315, 408	518	0.38	2.93 / 2.41	0.52	182/145/402	-5.39/-2.79	2.71
OIDBQx	287, 315, 411	534	0.31	2.88 / 2.39	0.49	198/146/398	-5.26/-2.75	2.68
ISBQx	276, 402	511	0.35	2.91 / 2.40	0.51	284/165/418	-5.41/-2.76	2.75

[a]absorption maxima in CH_2Cl_2 solution; [b]emission maxima in CH_2Cl_2 solution; [c]PL quantum yield in degassed CH_2Cl_2 solution; [d]singlet and triplet energy in Zeonex 1% (w/w) film; [e]singlet-triplet energy splitting in Zeonex 1% (w/w) film; [f]crystallisation (T_c), glass transition (T_g) and decomposition (T_d) temperatures determined by DSC and TGA measurements; [g]determined by cyclic voltammetry in CH_2Cl_2; [h]optical energy gap in CH_2Cl_2.

suppression of non-radiative decay playing an important role in enabling the long-lived emissions.

Although the iminostilbene intuitively appears more rigid than iminostilbene, the authors speculate that in fact the iminostilbene is relatively free to interconvert between chiral conformations, thus giving a fluttering motion. However, the singlet-triplet energy gap is still sufficient to allow thermal energy to partially up-convert the triplet states, and this is the reason why simultaneous TADF and RTP emissions were observed for derivatives of the iminodibenzyl compounds.

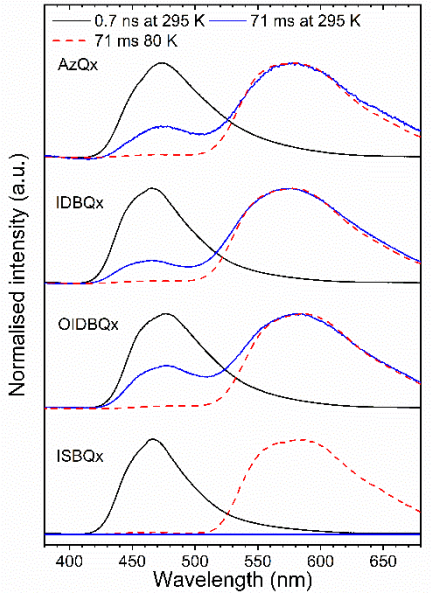

Fig 5. Prompt fluorescence (black solid line), room temperature phosphorescence and TADF (blue solid line), low temperature phosphorescence (red dashed line) spectra of molecular dispersions of the compounds in Zeonex.

The existence of TADF and absence of triplet-triplet annihilation was evidenced by the linear dependence of the intensity of the delayed fluorescence emission with laser dose, e.g. the slope of DF intensity vs. excitation power is equal 1 in log-log scale (see **Fig 6a** and **Fig 6c** and **Fig S13, S14** in the SI).[14] In general, the ratio between TADF and RTP correlates with the $\Delta E_{S\text{-}T}$, and in this respect the largest contribution of TADF was observed for OIDBQx. The ratio of intensities of RTP and TADF does not change with delay time for OIDBQx, which is also evidenced by monoexponential decay. This observation shows that both emissions originate from the same excited triplet state and both arrive from the same population of excited states. TADF+RTP dual emission of the derivatives of iminodibenzyl is strong and easily noticeable as a yellow-greenish afterglow. Furthermore, the lifetime of the TADF+RTP emission is relatively long, spanning from 51 ± 3 ms for AzQx to a remarkable 128 ± 10 ms for OIDBQx (see **Fig S9-S11** in the SI).

Such a behaviour can be explained by the suppression of the non-radiative decay of the triplet state and by substantial triplet formation yields. The non-bonding orbitals, such as those present in the donor unit, predetermine high triplet formation yields, due to the creation of n-π* transitions, which induce strong spin-orbit coupling, according to El-Sayed's rule. ~~However, the iminostilbene moiety does not support long-lived triplet emissions. This is likely to be caused by enhanced non-radiative decay affecting the ISB.~~ Both non-radiative decay and RISC process affect the iminodibenzyl derivatives, which is evidenced by substantially longer phosphorescence lifetimes observed at 80 K compared to the lifetime of TADF+RTP emissions recorded at 295 K. Remarkably, this is not the case in OIDBQx, where the two emissions show lifetimes that are statistically insignificantly different at different temperature (see **Fig S11** in the SI). The methoxy substitution not only stabilises the triplet state but appears to induce the largest triplet formation yield; in turn the TADF+RTP emission is the most efficient for OIDBQx. This can be caused either by inducing a larger contribution of the non-bonding pairs to the excited state by the introduction of the methoxy groups or by the fact that the $\Delta E_{S\text{-}T}$ is the smallest (which improves the coupling of the S_1 and T_1 states).

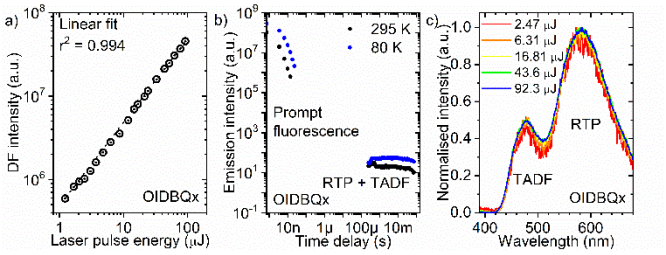

Fig 6. a) Power dependence of delayed fluorescence of OIDBQx at 295 K; b) photoluminescence decay transients of OIDBQx at 295 and 80 K; c) delayed fluorescence and room temperature phosphorescence spectra recorded at 295 K with various excitation pulse energy.

In mechanochromic materials increasing the strength of acceptor leads to stronger mechanochromism.[16] Interestingly, OIDBQx displays reversible luminescence changes upon applying external stress (**Fig 7**). The initial powder demonstrated greenish-blue emission with λ_{max} = 494 nm. Through grinding the initial powder with a spatula the emission broadened and red-shifted to 522 nm. The initial state was restored by exposure to CH_2Cl_2 vapour for 5 min. The vapour-treated form produced an emission spectrum nearly identical to that of the initial powder (λ_{max} = 495 nm). Neat film showed a similar emission spectrum to that of the ground

powder. In comparison with powder XRD data, initial and fumed forms appeared to be crystalline, whereas ground and neat film were amorphous (**Fig S16**). Additionally, in ground form and neat film the prompt fluorescence lifetimes were longer than in the initial and fumed forms (**Table 1 SI**). This implies stronger charge transfer character of the singlet excited state in the amorphous forms. In contrast, insignificant changes were observed in the emission of IDBQx under grinding. The photoluminescence maximum shifted from 495 nm to 499 nm. These results indicate that increasing the strength of the electron donor by methoxylation of IDB can increase colour contrast upon the application of external stimuli, in agreement with previous work.[14]

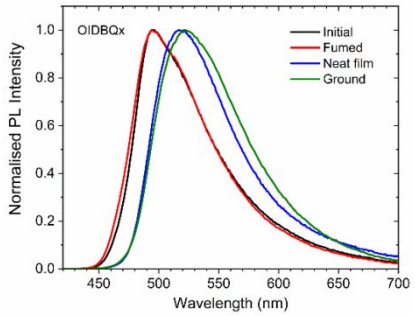

Fig 7. PL spectra of OIDBQx in different forms. Neat film obtained by drop casting.

In summary, we have designed and synthesised four new derivatives of quinoxaline-containing iminodibenzyl and iminostilbene moieties and studied their photophysical properties. These luminophores showed room temperature delayed fluorescence and phosphorescence, despite having a large singlet-triplet energy gap. An increase of the dipole moment of the iminodibenzyl derivative containing methoxy groups caused mechanochromic luminescent behaviour. The lifetime of room-temperature phosphorescence was found to increase through the introduction of a phenyl spacer between the donor and acceptor moieties and further increased by substitution of the iminodibenzyl moiety with methoxy groups. The investigations revealed that a twisted iminodibenzyl is a promising donor to suppress non-radiative decay. The observation of room temperature phosphorescence implies efficient spin orbit coupling to produce a sufficient triplet formation yield and to help to overcome radiationless decay from triplet excited states via shortening of the radiative triplet decay.

Conflicts of interest

There are no conflicts to declare.

Acknowledgments

This work was supported by the project EXCILIGHT, funded by the European Union's Horizon 2020 Research and Innovation Programme under grant agreement no. 674990. We thanks Dr Nils Trapp (Dep. of Chemistry and Applied Biosc., ETH Zürich) for the help of single crystal XRD analysis. We also thank Dr Algirdas Lazauskas (Inst. of Materials Science, Kaunas University of Technology) for assistance with PXRD measurements.

Notes and references

1- (a) P. Lehner, C. Staudinger, S. M. Borisov and I. Klimant, *Nat. Commun.*, 2014, **5**, 4460. (b) R. I. Dmitriev, A. V. Kondrashina, K. Koren, I. Klimant, A. V. Zhdanov, J. M. P. Pakan, K. W. McDermott and D. B. Papkovsky, *Biomater. Sci.*, 2014, **2**, 853–866. (c) Y. Deng, D. Zhao, X. Chen, F. Wang, H. Song and D. Shen, *Chem. Commun.*, 2013, **49**, 5751–5753.

2- M. Quaranta, S. M. Borisov and I. Klimant, *Bioanal. Rev.,* 2012, **4**, 115– 157.

3- (a) D. Lee, O. Bolton, B. C. Kim, J. H. Youk , S. Takayama and J. Kim, *J. Am. Chem. Soc.*, 2013, **135**, 6325. (b) D. Li, F. Lu, J. Wang, W. Hu, X.-M. Cao, X. Ma and H. Tian, *J. Am. Chem. Soc.*, 2018, **140**, 1916.

4- (a) Y. Shoji, Y. Ikabata, Q. Wang, D. Nemoto, A. Sakamoto, N. Tanaka, J. Seino, H. Nakai and T. Fukushima, *J. Am. Chem. Soc.,* 2017, **139**, 2728 (b) P. Pander, A. Swist, R. Motyka, J. Soloducho, F. B. Dias and P. Data, *J. Mater. Chem. C,* 2018*,* **6***,* 5434-5443*.* (c) X. Ma, C. Xu, J. Wang and H. Tian, *Angew. Chem. Int. Ed.,* 2018, **57**, 1.

5- (a) Z. Yang, Z. Mao, Z. Xie, Y. Zhang, S. Liu, J. Zhao, J. Xu, Z. Chi and M. P. Aldred, *Chem. Soc. Rev.*, 2017, **46**, 915. (b) G. Grybauskaite-Kaminskiene, K. Ivaniuk, G. Bagdziunas, P. Turyk, P. Stakhira, G. Baryshnikov, D. Volyniuk, V. Cherpak, B. Minaev, Z. Hotra, H. Agren and J. V. Grazulevicius, *J. Mater. Chem. C*, 2018, **6**, 1543-1550. (c) T. Matulaitis, P. Imbrasas, N. A. Kukhta, P. Baronas, T. Buciunas, D. Banevicius, K. Kazlauskas, J. V. Grazulevicius and S. Jursenas, *J. Phys. Chem. C*, 2017, **121**, 23618–23625.

6- (a) C. Li, Y. Wang, D. Sun, H. Li, X. Sun, D. Ma, Z. Ren and S. Yan, *ACS Appl. Mater. Interfaces*, 2018, **10**, 5731. (b) S. Shao, J. Hu, X. Wang, L. Wang, X. Jing and F. Wang, *J. Am. Chem. Soc.*, 2017, **139**, 17739.

7- (a) M. Y. Wong and E. Zysman-Colman, *Adv. Mater.,* 2017, 1605444. (b) P. Schrogel, A. Tomkevicienė, P. Strohriegl, S. T. Hoffmann, A. Kohlerb and C. Lennartz, *J. Mater. Chem.*, 2011, **21**, 2266-2273.

8- (a) Z. Wang and W. G. McGimpsey, *J. Phys. Chem.*, 1993, **97**, 9668–9672. (b) S. Dollinger, S. Löber, R. Klingenstein, C. Korth and P. Gmeiner, *J. Med. Chem.*, 2006, **49**, 6591 (c) L. J. Kricka and A. Ledwith, *Chem. Rev.*, 1974, **74**, 101.

9- C. Dardonville, M. L. Jimeno, I. Alkorta and J. Elguero, *Org. Biomol. Chem.*, 2004, **2**, 1587-1591.

10- M.-H. Ho, C.-M. Chang, T.-Y. Chu, T.-M. Chen and C. H. Chen, *Org. Electron.*, 2008, **9**, 101–110.

11- C. Sun, X. Ran, X. Wang, Z. Cheng, Q. Wu, S. Cai, L. Gu, N. Gan, H. Shi, Z. An, H. Shi and W. Huang, *J. Phys. Chem. Lett.*, 2018, **9**, 335.

12- (a) Z. Mao, Z. Yang, Y. Mu, Y. Zhang, Y. F. Wang, Z. Chi, C. C. Lo, S. Liu, A. Lien and J. Xu, *Angew. Chem. Int. Ed.,* 2015, **54**, 6270–6273. (b) L. Xiao, Y. Wu, J. Chen, Z. Yu, Y. Liu, J. Yao and H. Fu, *J. Phys. Chem. A*, 2017, **121**, 8652 (c) D. Li, F. Lu, J. Wang, W. Hu, X.-M. Cao, X. Ma and H. Tian, *J. Am. Chem. Soc.*, 2018, **140**, 1916.

13- (a) R. Huang, J. Avo, T. Northey, E. Chaning-Pearce, P. L. D. Santos, J. S. Ward, P. Data, M. K. Etherington, M. A. Fox, T. J. Penfold, M. N. Berberan-Santos, J. C. Lima, M. R. Bryce and F. B. Dias, *J. Mater. Chem. C*, 2017, **5**, 6269. (b) I. Bhattacharjee, N. Acharya, H. Bhatia and D. Ray, *J. Phys. Chem. Lett.*, 2018, **9**, 2733. (c) Y. Takeda, T. Kaihara, M. Okazaki, H. Higginbotham, P. Data, N. Tohnai and S. Minakata, *Chem. Commun.*, 2018, **54**, 6847–6850.

14- R. Pashazadeh, P. Pander, A. Lazauskas, F. B. Dias and J. V. Grazulevicius, *J. Phys. Chem. Lett.*, 2018, **9**, 1172–1177.

15- (a) O. Vybornyi, N. J. Findlay and P. J. Skabara, *J. Vis. Exp*., 2017, (128), e56501. (b) W. Huang and S. L. Buchwald, *Chem.–Eur. J*., 2016, **22**, 14186–14189.

16- T. Jadhav, B. Dhokale and R. Misra, *J. Mater. Chem. C*, 2015, **3**, 9063-9068.

Graphical abstract

Dual emission (TADF+RTP) and mechanochromism have been obtained using an iminodibenzyl-quinoxaline-iminodibenzyl scaffold.

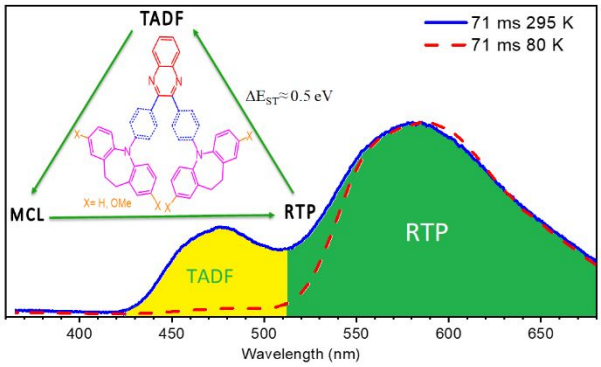

SI

An Iminodibenzyl-Quinoxaline-Iminodibenzyl Scaffold as a Mechanochromic and Dual Emitter: Donor and Bridge Effects on Optical Properties

Ramin Pashazadeh,[a] Piotr Pander,[b] Audrius Bucinskas,[a] Peter J. Skabara,[c] Fernando B. Dias,*[b] Juozas V. Grazulevicius*[a]

[a.] Department of Polymer Chemistry and Technology, Kaunas University of Technology, Kaunas, Lithuania.
[b.] Department of Physics, University of Durham, South Road DH1 3LE, Durham, UK.
[c.] WestCHEM, School of Chemistry, University of Glasgow, Glasgow G12 8QQ, UK

Emails: juozas.grazulevicius@ktu.lt , f.m.b.dias@durham.ac.uk

1. General methods:

^{1}H and ^{13}C NMR spectroscopy was carried out on a Bruker Avance 400 NMR spectrometer at 400 MHz and 100 MHz, respectively; δ in ppm. The residue signals of the solvents were used as internal standards. Attenuated total reflection infrared (ATR IR) spectra were recorded using a Bruker VERTEX 70 spectrometer. MS data was recorded on UPLC-MS Acquity Waters SQ Detector 2.

Absorption spectra of 10^{-5} M solutions or films were measured with Perkin Elmer Lambda 35 spectrometer or UV-3600 double beam spectrophotometer (Shimadzu). Photoluminescence (PL) spectra of 10^{-5} M solutions, films, and powders were recorded using Edinburgh Instruments' FLS980 Fluorescence Spectrometer or FluoroMax-3 fluorescence spectrometer (Jobin Yvon). Phosphorescence, prompt fluorescence (PF), and delayed fluorescence (DF) spectra and fluorescence decay curves were recorded using nanosecond gated luminescence and lifetime measurements (from 400 ps to 1 s) using either third harmonics of a high energy pulsed Nd:YAG laser emitting at 355 nm (EKSPLA) or a N_2 laser emitting at 337 nm. Emission was focused onto a spectrograph and detected on a sensitive gated iCCD camera (Stanford Computer Optics) having sub-nanosecond resolution. PF/DF time resolved measurements were performed by exponentially increasing gate and integration times. Temperature-dependent experiments were conducted using a continuous flow liquid nitrogen cryostat (Janis Research) under nitrogen atmosphere, while measurements at room temperature were recorded in vacuum in the same cryostat. Photoluminescence quantum yield has been recorded using Fluorescein in 0.1 M NaOH as a standard (Φ = 0.90). Power dependence data was fitted using a linear espression: $y = a \cdot x$ for linear relation.

The single crystals of compounds were obtained from the mixture of solvents (DCM, acetone, hexane). Yellow color single crystals were mounted on the glass capillary using glue. The crystallographic analysis was performed employing XtaLAB mini diffractometer (Rigaku) with graphite monochromated Mo Kα (λ=0.71075 Å) X-ray source. The measurements were performed at the temperature of 293 K.

Thermogravimetric analysis (TGA) was performed on a Metter TGA/SDTA851e/LF/1100 apparatus at a heating rate of 20°C/min under nitrogen atmosphere. Differential scanning calorimetry (DSC) measurements were done on a DSC Q 100 TA Instrument at a heating rate of 10°C/min under nitrogen atmosphere

Cyclic voltammetry (CV) measurements were carried out with Eco Chemie Company's AUTOLAB potentiostat "PGSTAT20" and a glassy carbon working electrode in a three electrode cell. The measurements were performed in 0.1 M nBu_4NPF_6 solution in anhydrous dichloromethane at room temperature under nitrogen atmosphere.

The crystallographic nature of the powder materials was determined using D8 Discover X-ray diffractometer (Bruker AXS GmbH) with Cu Kα (λ= 1.54 Å) X-ray source. Parallel beam geometry with 60 mm Göbel mirror (i.e. X-ray mirror on a high precision parabolic surface) was used. This configuration enables transforming the divergent incident X-ray beam from a line focus of the X-ray tube into a parallel beam that is free of Kβ radiation. Primary side also had a Soller slit with an axial divergence of 2.5 º and a slit of 1 mm. The secondary side had a LYNXEYE (1D mode) detector with an opening angle of 2.160 º and slit opening of 6.0 mm. X-ray generator voltage and current was 40.0 kV and 40 mA, respectively. Coupled 2θ/θ scans were performed in the range of 3.0-60.0 º with a step size of 0.028 º, time per step of 19.2 s and auto-repeat function enabled. Processing of the resultant diffractograms was performed with DIFFRAC.EVA software.

2. Synthetic procedure:

1,2-dicholoro quinoxaline (I), 2,3-bis(4-bromophenyl)quinoxaline (V) and 2,8-dibromo-5*H*-dibenzo[*b,f*]azepine are prepared by the reported method in the literature.[1-3]

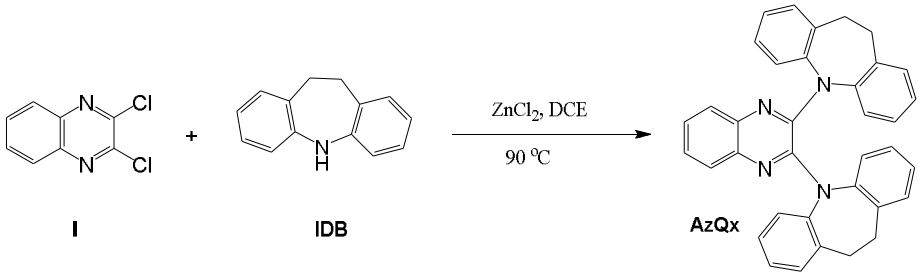

Figure S1: Synthetic procedure for preparation of AzQx

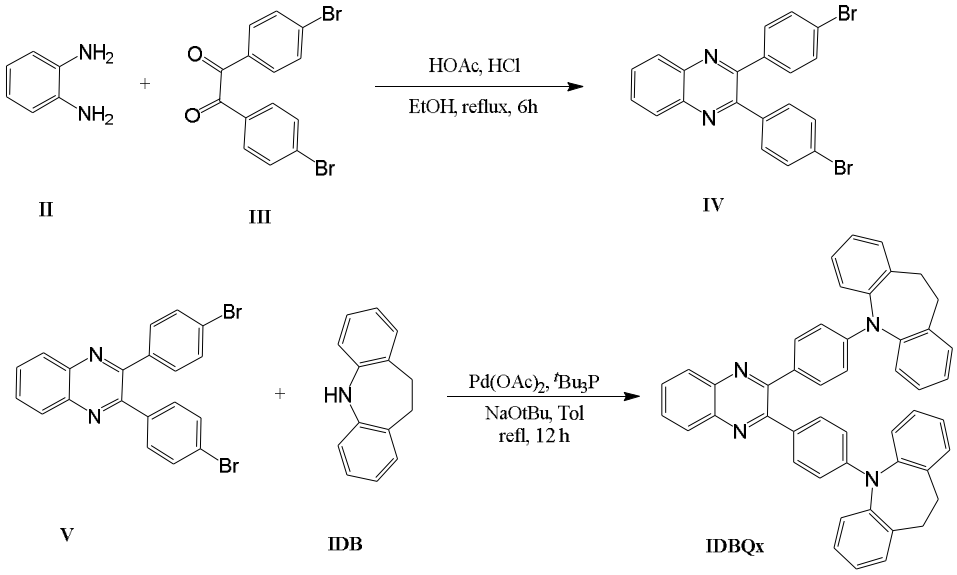

Figure S2: Synthesis routes for preparation of IDBQx

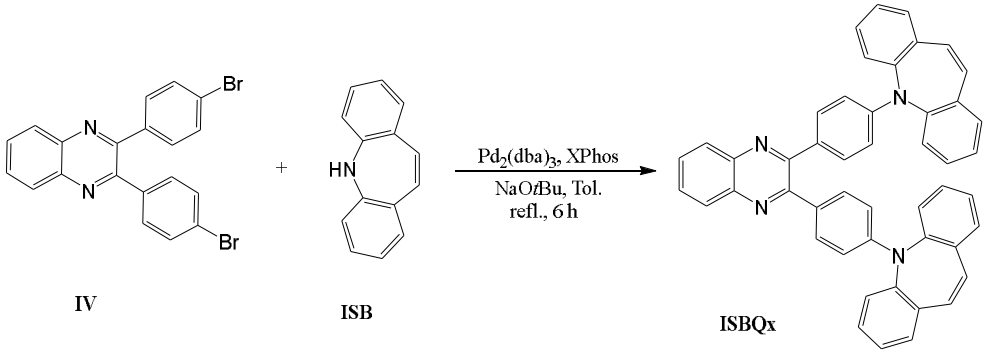

Figure S3: Synthesis procedure to generate ISBQx

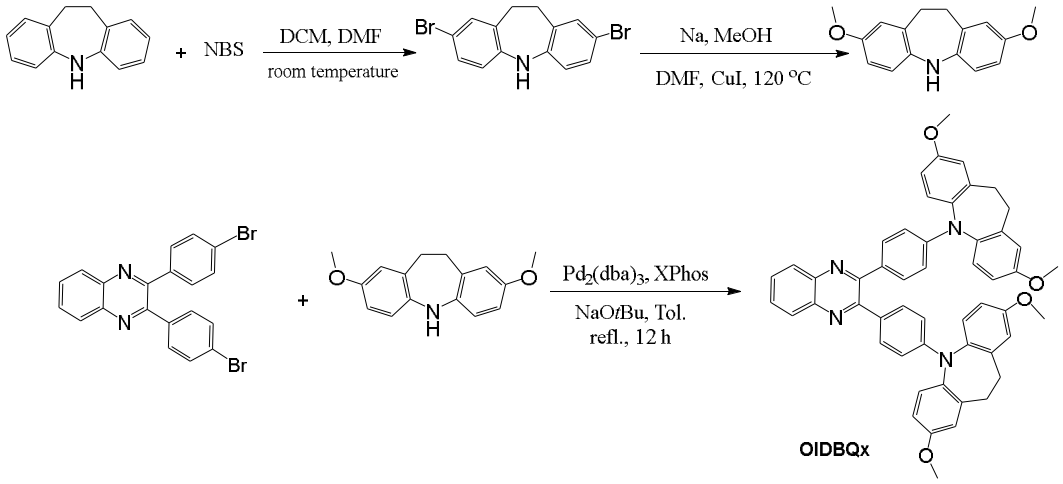

Figure S4: Synthesis routs for generation of OIDBQx

Synthesis of 2,8-dibromo-10,11-dihydro-5*H*-dibenzo[*b,f*]azepine:

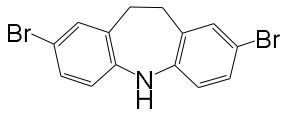

Iminodibenzyl (5 mmol) was added to a solution of DCM (15 mL) in silica gel (2 g). After stirring for 5min *N*-bromosuccinimide (NBS, 10 mmol, 1.78 g) dissolved in DCM:DMF (25:15 mL) was added dropwise and stirred for 1 h at room temperature. Reaction mixture filtered and washed with DCM. The crude product were purified by column chromatography (n-hexane/EtOAc 10:1) to give the white powder. Yield (1.10 g, 63%). ^{1}H NMR (400 MHz, DMSO-d_6): δ_H = 8.58 (1H, s, NH), 7.2 (2H, s, CH), 7.19 (2H, d, ^{3}J= 9.4 Hz, CH), 6.91 (2H, d, ^{3}J= 9.2 Hz, CH), 2.92 (4H, s, CH_2) ppm. ^{13}C NMR (100 MHz, DMSO-d_6): δ_C = 142.2, 132.8, 130.6, 129.6, 120.4, 110.1, 34.5 ppm. MS, m/z = 350 ([M-H]$^+$, 36%) 353 ([M+2, 100%]$^+$).

Synthesis of 2,8-dimethoxy-10,11-dihydro-5*H*-dibenzo[*b,f*]azepine:

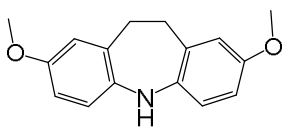

Na (3.2 g) was dissolved in dry MeOH (25 mL) under N_2 at 0 °C, and then 2,8-dibromo-10,11-dihydro-5*H*-dibenzo[*b,f*]azepine (1.1 g, 3.1 mmol), CuI (1.18 g, 6.2 mmol) and DMF (30 mL) at 125 °C for 12 h were stirred. After cooling to room temperature, the mixture was filtered through silica gel with EtOAc, and evaporated and washed with water and dried over Na_2SO_4. The combined organic layers were purified by

column chromatography on silica gel (n-Hexane/EtOAc 6:1) to afford the white product. Yield (616 mg, 78%). ^{1}H NMR (400 MHz, DMSO-d_6): δ_H = 7.66 (1H, s, NH), 6.85 (2H, d, ^{3}J= 8.6 Hz, CH), 6.64-6.59 (4H, m, CH), 3.66 (6H, s, OMe), 2.92 (4H, s, CH_2) ppm. ^{13}C NMR (100 MHz, DMSO-d_6): δ_C = 152.2, 138.0, 129.0, 119.1, 115.6, 112.8, 55.6, 34.7 ppm. MS, m/z = 254 ([M]$^+$, 100%). HRMS (ESI): calcd for $C_{16}H_{17}NO_2$ ([M+H]$^+$): 255.1259; found: 255.1253.

Synthesis of 2,3-bis(4-(10,11-dihydro-5*H*-dibenzo[*b,f*]azepin-5-yl)phenyl)quinoxaline (IDBQx):

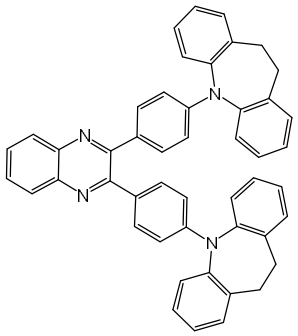

Procedure A: Two neck flask was charged with Iminodibenzyl (468 g, 2.4 mmol), 2,3-bis(4-bromophenyl)quinoxaline (438 mg, 1 mmol) and NaO*t*-Bu (250 mg), evacuated and backfilled with N_2 for 3 times. Then, $Pd(OAc)_2$ (22 mg, 0.01 mmol, 10 mol%) and tBu$_3$P (25 mg, 0.12 mmol, 12 mol%) were added under flow on nitrogen, and followed by charging with 10 mL of toluene. Reaction stirred for overnight at reflux. After cooling to room temperature, the mixture was filtered through silica gel by $CHCl_3$, and concentrated in vacuum. The crude product were isolated by column chromatography on silica gel (n-hexane/EtOAc 4:1) to afford yellow powder. Yield (454 mg, 68%). ^{1}H NMR (400 MHz, $CDCl_3$): δ_H = 7.98 (2H, dd, ^{3}J= 6.1 Hz, ^{4}J= 3.3 Hz, CH), 7.54 (2H, dd, ^{3}J= 6.4 Hz, ^{4}J= 3.4 Hz, CH), 7.34 (4H, d, ^{4}J= 7.6 Hz, CH), 7.25 (4H, d, ^{3}J= 8.8 Hz, CH), 7.20-7.12 (12H, m, CH), 6.44 (4H, d, ^{3}J= 8.8 Hz, CH), 2.89 (8H, s, CH_2) ppm. ^{13}C NMR (100 MHz, $CDCl_3$): δ_C = 153.4, 149.6, 143.2, 140.7, 138.2, 130.9, 130.6, 129.9, 129.0, 128.7, 127.3, 127.1, 112.3, 30.7 ppm. MS, m/z = 668 ([M]$^+$, 19%), HRMS (ESI) calcd for $C_{48}H_{36}N_4$ ([M+H]$^+$): 669.3013; found: 669.3013.

Synthesis of 2,3-bis(4-(5*H*-dibenzo[*b,f*]azepin-5-yl)phenyl)quinoxaline (ISBQx):

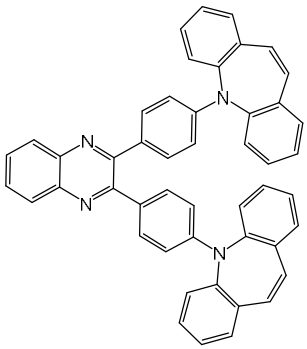

Procedure B: Two neck flask was charged with iminostilbene (340 mg, 1.76 mmol), 2,3-bis(4-bromophenyl)quinoxaline (365 mg, 0.83 mmol) and NaO*t*-Bu (354 mg, 3.8 mmol), evacuated and backfilled with N_2 for 3 times. Then, $Pd_2(dba)_3$ (56 mg, 0.06 mmol, 7 mol%) and XPhos (40 mg, 0.08 mmol, 10 mol%) were added under flow on nitrogen, and followed by charging with 10 mL of toluene. Reaction stirred for 6 hours at reflux. After cooling to room temperature, the mixture was filtered through silica gel by $CHCl_3$, and concentrated in vacuum. The crude product were isolated by column chromatography on silica gel (n-hexane/EtOAc 5:1) to afford yellow powder. Yield (402 mg, 73%). ^{1}H NMR (400 MHz, $CDCl_3$): δ_H = 7.96 (2H, bs, CH), 7.54 (2H, dd, ^{3}J= 6.3 Hz, ^{4}J= 3.0 Hz, CH), 7.43 (2H, dd, ^{4}J= 3.8 Hz, CH), 7.36 (4H, d, ^{3}J= 7.6 Hz, CH), 7.32-7.28 (4H, m, CH), 7.13 (4H, d, ^{3}J= 8.8 Hz, CH), 6.70 (4H, s, CH) ppm. ^{13}C NMR (100 MHz, $CDCl_3$): δ_C = 153.1, 149.5, 142.7, 140.3, 136.2, 130.5, 130.3, 130.2, 130.1, 129.7, 129.1, 128.4, 127.2, 111.8 ppm. MS, m/z = 664 ([M]$^+$, 48%). HRMS (ESI) calcd for $C_{48}H_{32}N_4$ ([M+H]$^+$): 665.2700; found: 665.2706.

Synthesis of 2,3-bis(10,11-dihydro-5*H*-dibenzo[*b,f*]azepin-5-yl)quinoxaline (AzQx):

Due to twist boat conformation of IDB in this small molecule desymmetrization resulted in exhibiting 18 carbon peaks in ^{13}CNMR.

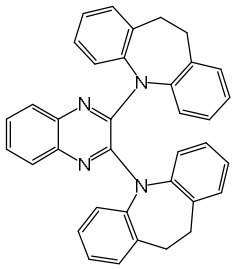

A mixture of iminodibenzyl (410 mg, 2.1 mmol) and 2,3-dichloroquinoxaline (198 mg, 1 mmol) dissolved in 7 mL DCE and and added $ZnCl_2$ (286 mg, 2.1 mmol) at 90 °C for 12 h. After completion, the reaction mixture was poured into 30 mL water, and organic products were extracted with DCM (3x15mL). The crude compound was purified by column chromatography (n-hexane/DCM 1:1) to afford yellow powder. Yield (93 mg, 18%). ^{1}H NMR (400 MHz, $CDCl_3$): δ_H = 8.03 (2H, dd, ^3J= 6.3 Hz, ^4J= 3.4 Hz, 2CH), 7.61 (2H, dd, ^3J= 6.3 Hz, ^4J= 3.4 Hz, 2CH), 7.35 (2H, d, ^4J= 2.1 Hz, CH), 7.09 (2H, dd, ^3J= 8.3 Hz, ^4J= 2.1 Hz, CH), 7.03-6.96 (4H, m, CH), 6.07 (2H, t, ^3J= 7.4 Hz, CH), 6.67 (2H, d, ^3J= 8.3 Hz, CH), 6.54 (2H, d, ^3J= 8.3 Hz, CH), 6.06 (2H, s, CH), 2.99 (8H, s, CH_2) ppm. ^{13}C NMR (100 MHz, $CDCl_3$): δ_C = 153.0, 142.9, 141.8, 140.9, 132.3, 130.6, 130.0, 129.2, 129.0, 128.8, 128.6, 128.0, 126.9, 119.9, 118.1, 117.4, 35.2, 34.9 ppm. MS, m/z = 516 ([M]$^+$, 51%). HRMS (ESI)) calcd for $C_{36}H_{282}N_4$ ([M+H]$^+$): 517.2387; found: 517.2390.

Synthesis of 2,3-bis(4-(2,8-dimethoxy-10,11-dihydro-5*H*-dibenzo[*b,f*]azepin-5-yl)phenyl)quinoxaline (OIDBQx):

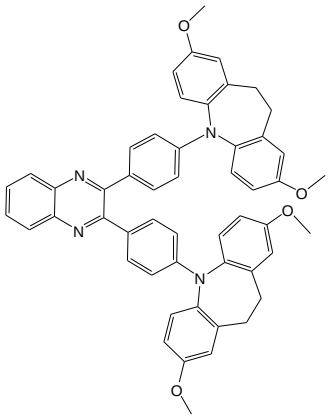

Prepared according to the procedure B, and organic products were extracted with DCM. The crude product was purified by column chromatography (n-hexane/DCM 1:1). Yield (490 mg, 75%). ^{1}H NMR (400 MHz, $CDCl_3$): δ_H = 7.95 (2H, dd, ^3J= 6.3 Hz, ^4J= 3.4 Hz, CH), 7.54 (2H, dd, ^3J= 6.3 Hz, ^4J= 3.4 Hz, CH), 7.25-7.21 (8H, m, CH), 6.73-6.70 (8H, m, CH), 6.40 (4H, d, ^3J= 8.9 Hz, CH), 3.72(12H, s, OMe), 2.84 (8H, s, CH_2) ppm. ^{13}C NMR (100 MHz, $CDCl_3$): δ_C = 158.3, 153.5, 150.4, 140.8, 139.3, 136.7, 130.7, 130.5, 128.8, 128.4, 115.6, 112.4, 112.2, 55.4, 30.9 ppm. MS, m/z = 788 ([M]$^+$, 1%). HRMS (ESI) calcd for $C_{52}H_{44}N_4O_4$ ([M+H]$^+$): 789.3435; found: 789.3440.

3. Electrochemical characterization:

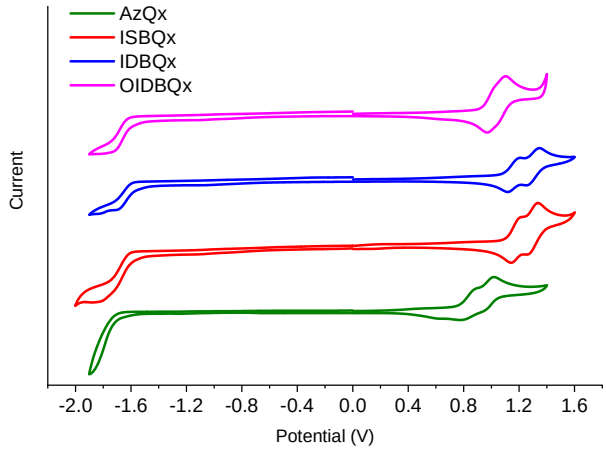

Figure S5. Oxidation and reduction potential of compounds in DCM recorded with cyclic voltammetry.

E_{HOMO} = - ($E^{1/0}{}_{1/2}$ (vs. Fc^+/Fc) +4.8), E_{LUMO} = - ($E^{0/1}$ (vs. Fc^+/Fc) + 4.8)

4. DSC and TGA Analyses:

Molecules with phenylene linkage demonstrated higher thermal stability and glass transition than AzQx. These desired behaviours can be ascribed to increasing of intermolecular interactions. In addition, AzQx did not show any melting point and attributed to its amorphous form.

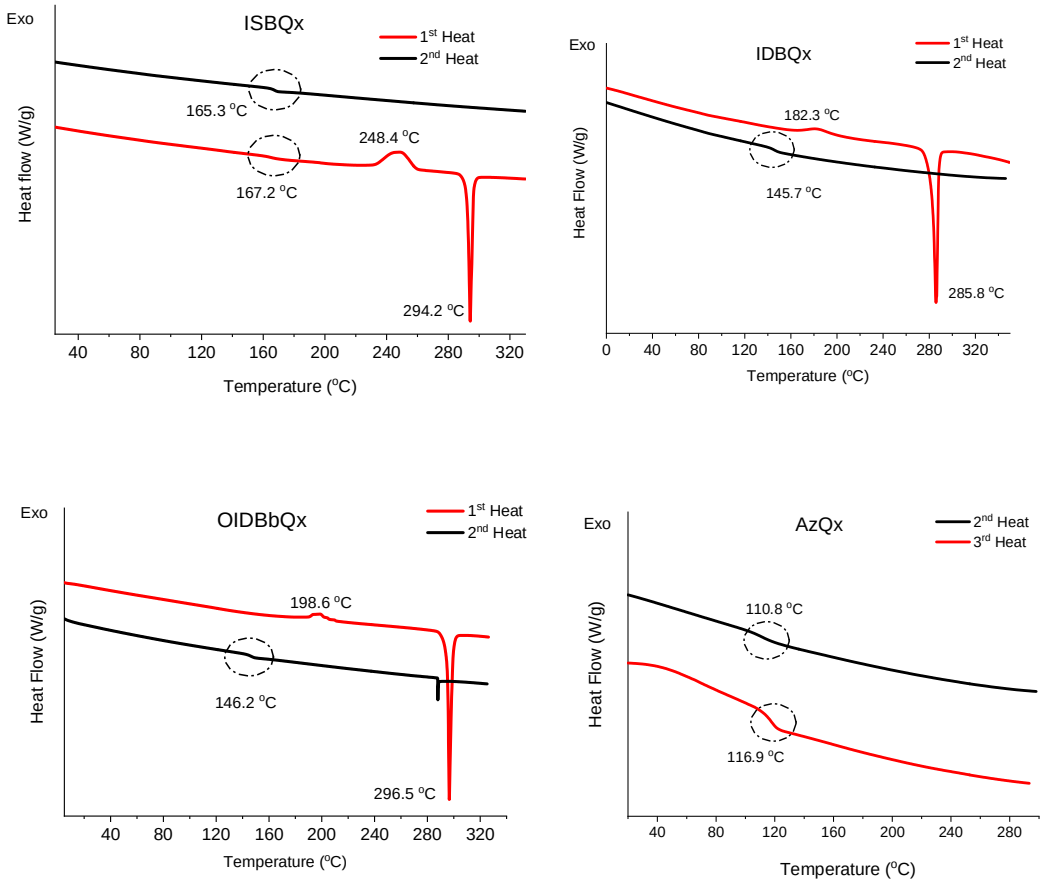

Figure S6. Differential scanning calomery analysis of samples.

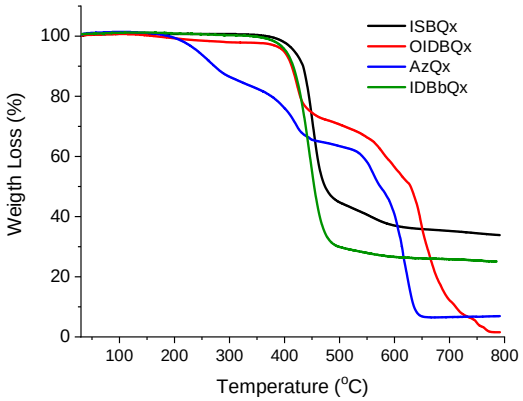

Figure S7. The TGA thermograms of materials (5% weight loss).

5. Photophysical characterization:

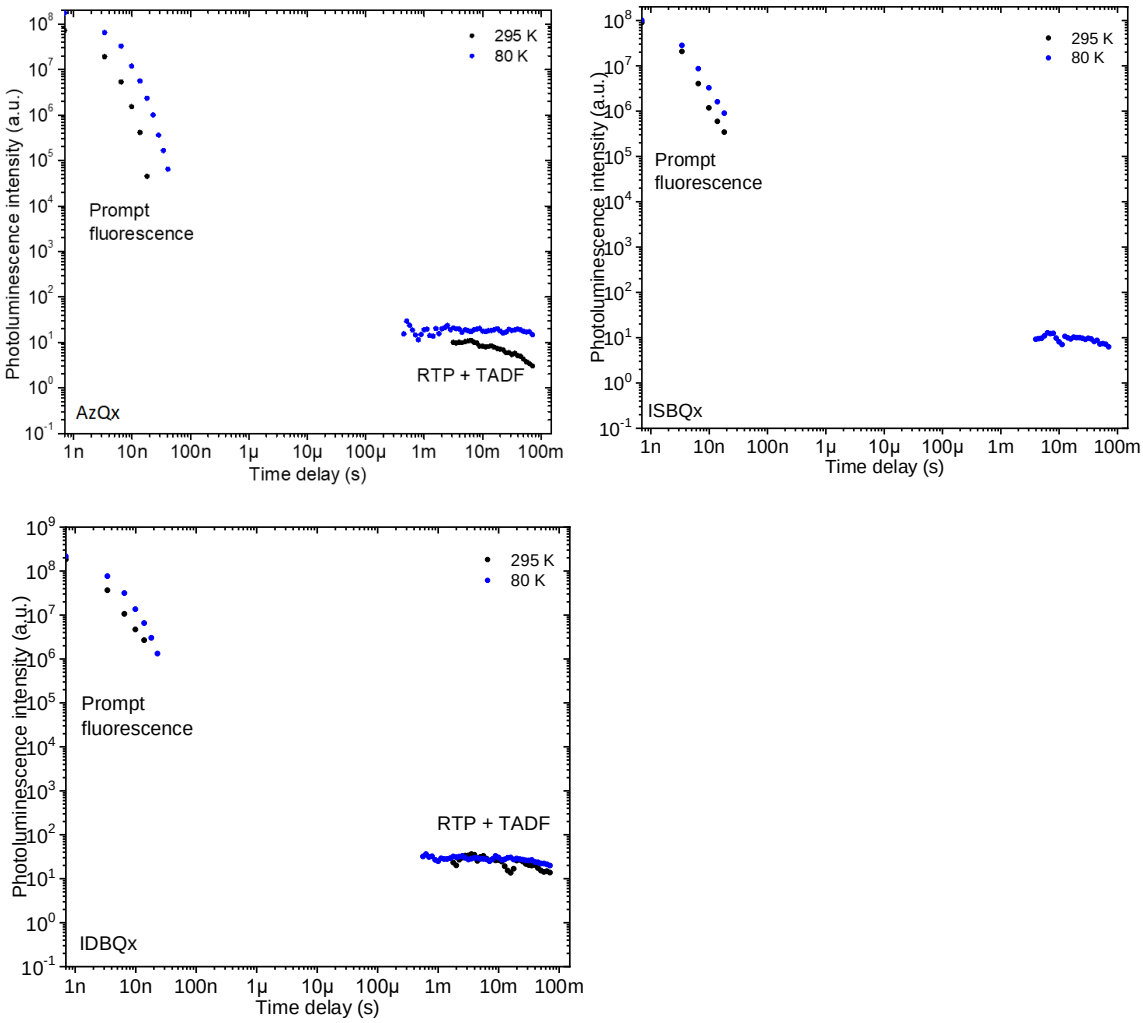

Figure S8. Photoluminescence decay transients at 80 and 295 K in Zeonex.

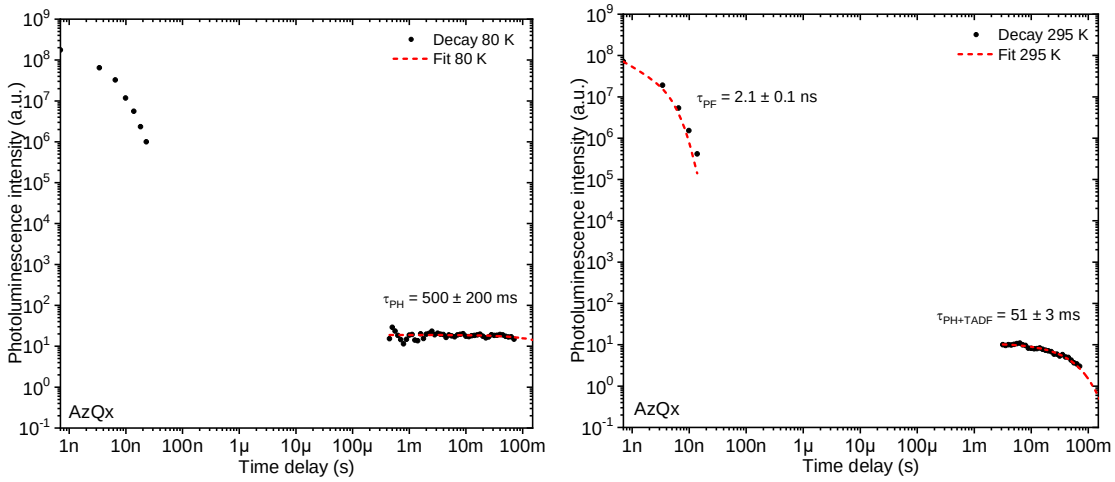

Figure S9. Photoluminescence decay transient fits of AzQx at 80 and 295 K in Zeonex.

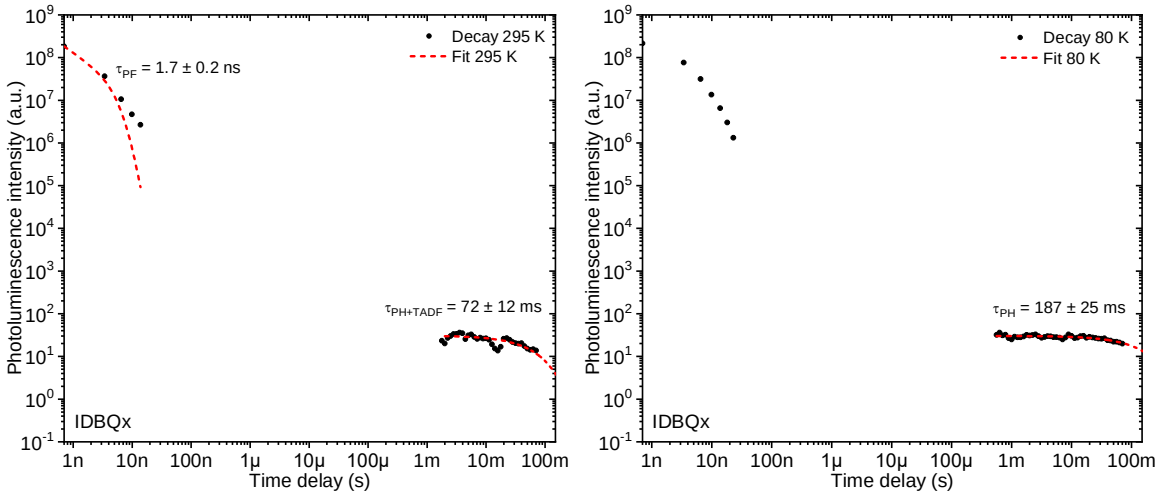

Figure S10. Photoluminescence decay transient fits of IDBQx at 80 and 295 K in Zeonex.

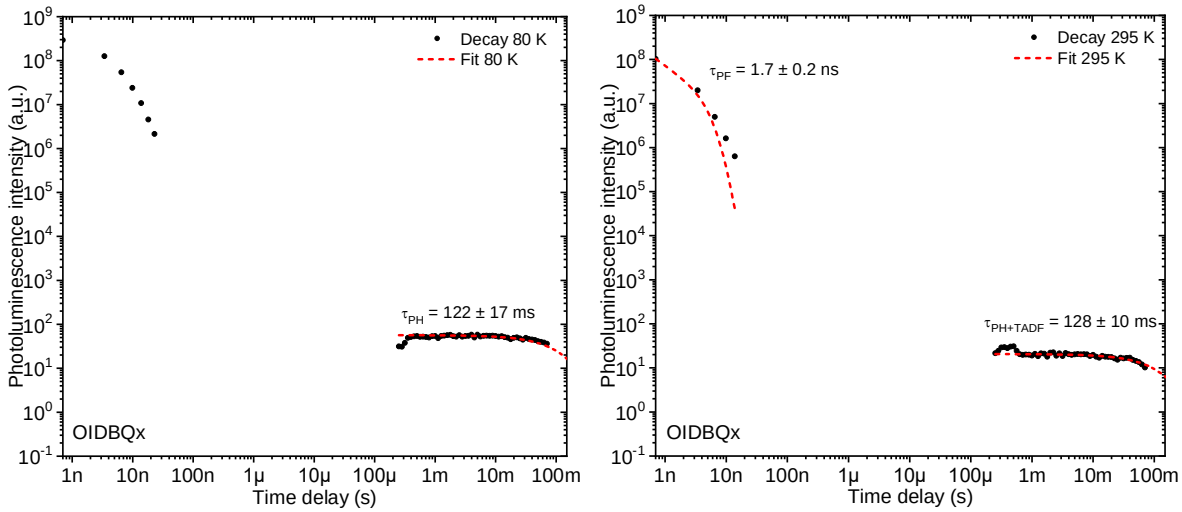

Figure S11. Photoluminescence decay transient fits of OIDBQx at 80 and 295 K in Zeonex.

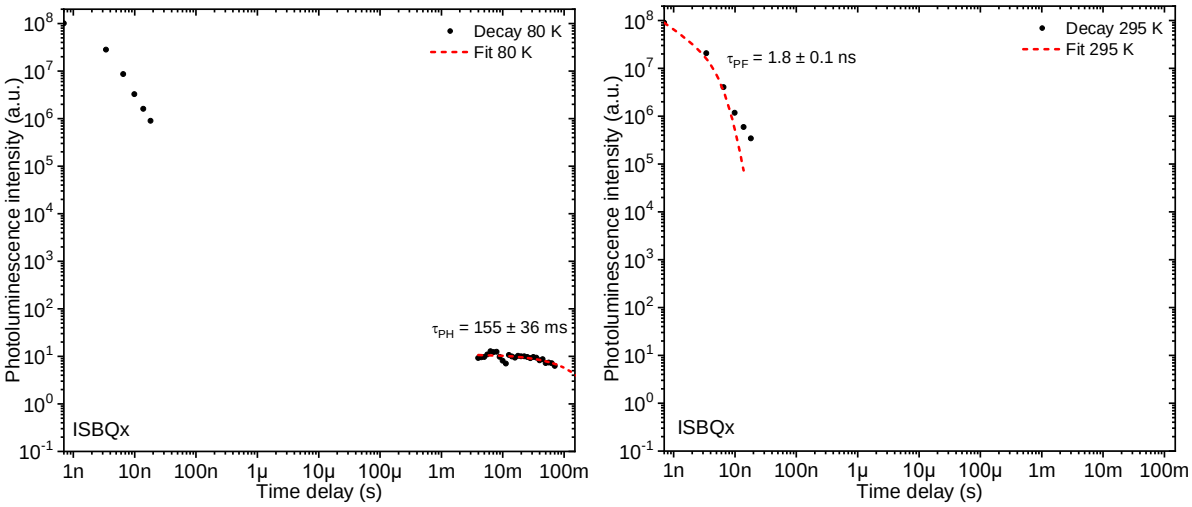

Figure S12. Photoluminescence decay transient fits of ISBQx at 80 and 295 K in Zeonex.

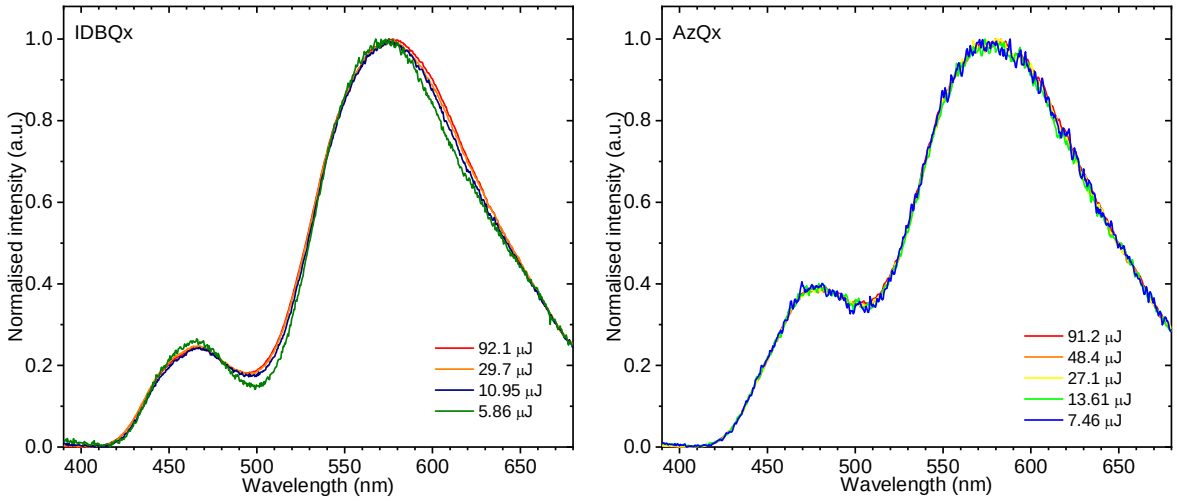

Figure S13. Delayed fluorescence and room temperature phosphorescence spectra at 295 K recorded with various excitation pulse energy.

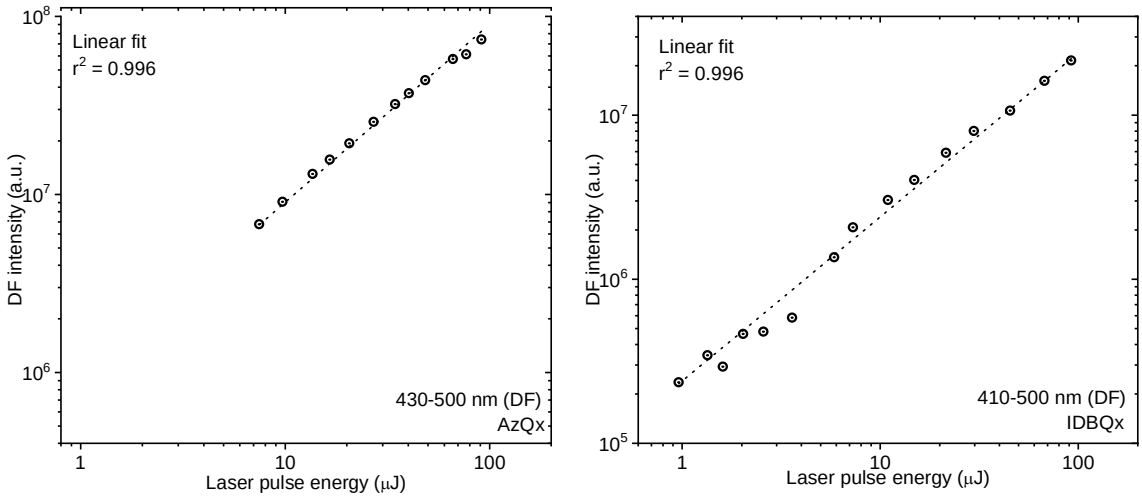

Figure S14. Laser fluence dependence of delayed fluorescence at room temperature in Zeonex.

6. Mechanochromic characteristics

Table S1 PL and decay time of OIDBQx under external stimuli

Sample (OIDBQx)	Initial	Ground	Fumed	Neat film
PL (nm)	494	522	495	518
τ_1 (ns)	0.21 (46.41%)	1.40 (70.83%)	0.32 (60.81%)	1.39 (72.86%)
τ_2 (ns)	1.67 (53.59%)	4.48 (29.15%)	1.72 (39.19%)	4.30 (27.14%)
X^2	1.07	1.06	1.07	1.03

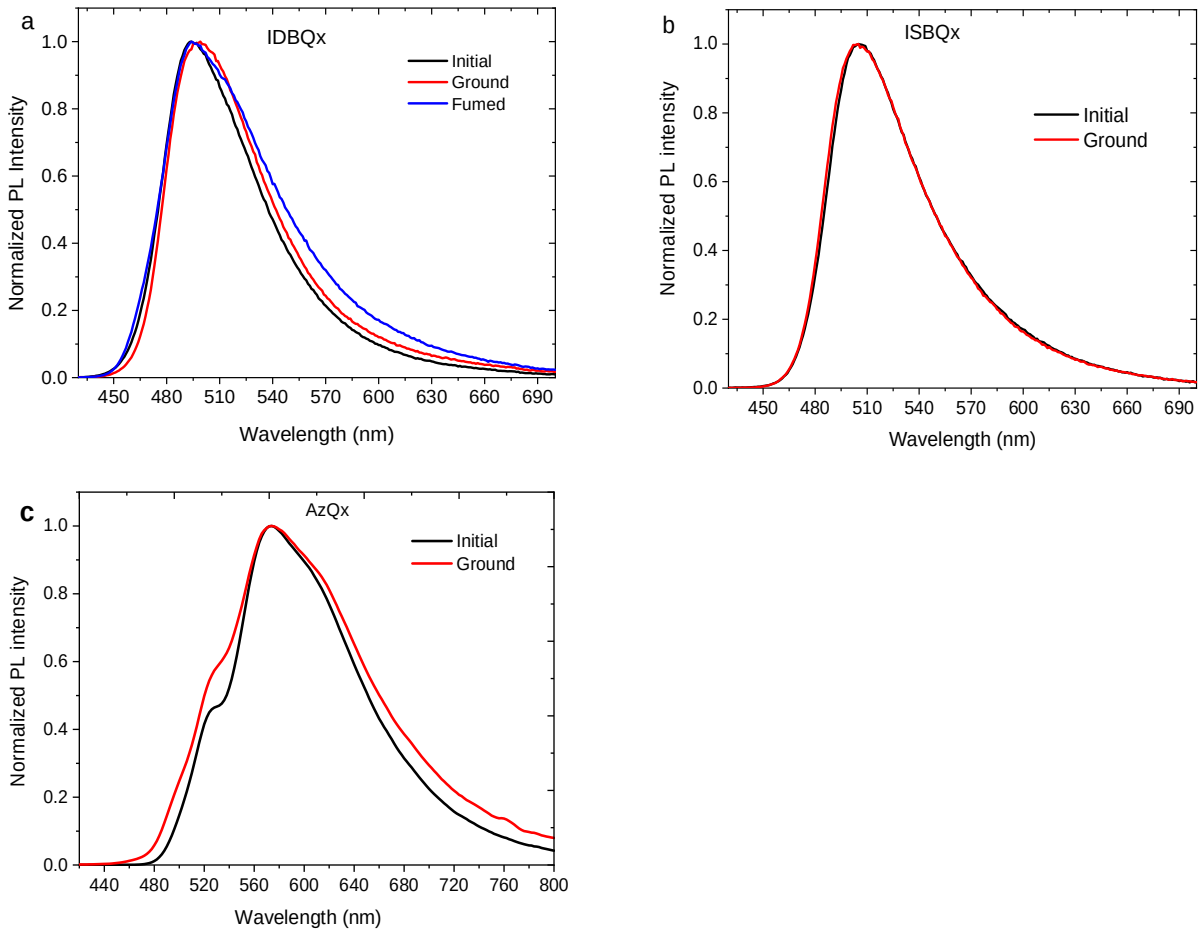

Figure S15. PL spectra of a) IDBQx and b) ISBQx and c) AzQx under external stimuli.

7. Powder XRD analyses:

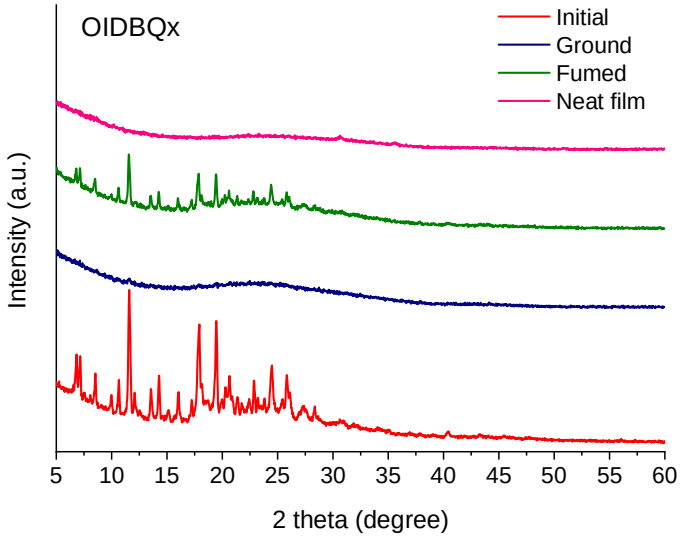

Figure S16. Powder Xray diffractogram of OIDBQx under application in initial form (-i), ground (-g), drop-cast film (-df) and after fumigation (-f).

8. Single crystal XRD analyses:

The crystallographic data is summarized in Table S2. Packing along a-axis is presented in Figure S15 and S16. The crystallographic data for structures IDBQx and ISBQx reported in this paper have been deposited in Cambridge Crystallographic Data Centre with CCDC no 1861441-1861442. The copies of data can be obtained free of charge on application to CCDC.(The Cambridge Structural Database (CSD)- The Cambridge Crystallographic Data Centre (CCDC), (http://www.ccdc.cam.ac.uk/solutions/csd-system/components/csd/). Calculations/visualizations were performed using the OLEX2 crystallographic software[3] package except for refinement, which was performed using SHELXL. [4,5] For molecule ISBQx solvent mask procedure was used. Anisotropic thermal parameters were assigned to all nonhydrogen atoms. The hydrogens were included in the structure factor calculation at idealized positions by using a riding model and refined isotropically.

Table S1. Structure data of IDBQx and ISBQx

	IDBQx	ISBQx
Empirical Formula	$C_{48}H_{36}N_4$. CH_3COCH_3	$C_{48}H_{32}N_4$
Crystal Dimensions (mm)	0.6x0.2x0.2	0.2x0.1x0.1
Crystal System	triclinic	triclinic
Space group	P-1	P-1
Cell angles (°)	α= 102.079(9) β= 93.931(9) γ= 93.152(9)	α= 78.98(2) β= 81.21(2) γ= 67.65(3)
Cell length (Å)	*a* =11.1633(11) *b* =12.2381(14) *c* =15.3155(16)	*a* = 12.135(4) *b* = 12.225(3) *c* = 17.067(4)
Cell volume ($Å^3$)	2036.1(4)	2289.4(12)
Z value	9	10
D_{calc} (g cm^{-3})	1.186	0.964
F (000)	768	696
λ (Mo *K*α) (Å)	0.71073	0.71073
h_{max}, k_{max}, l_{max}	12, 15, 18	14, 12, 21
Temperature (K)	293(2)	293(2)

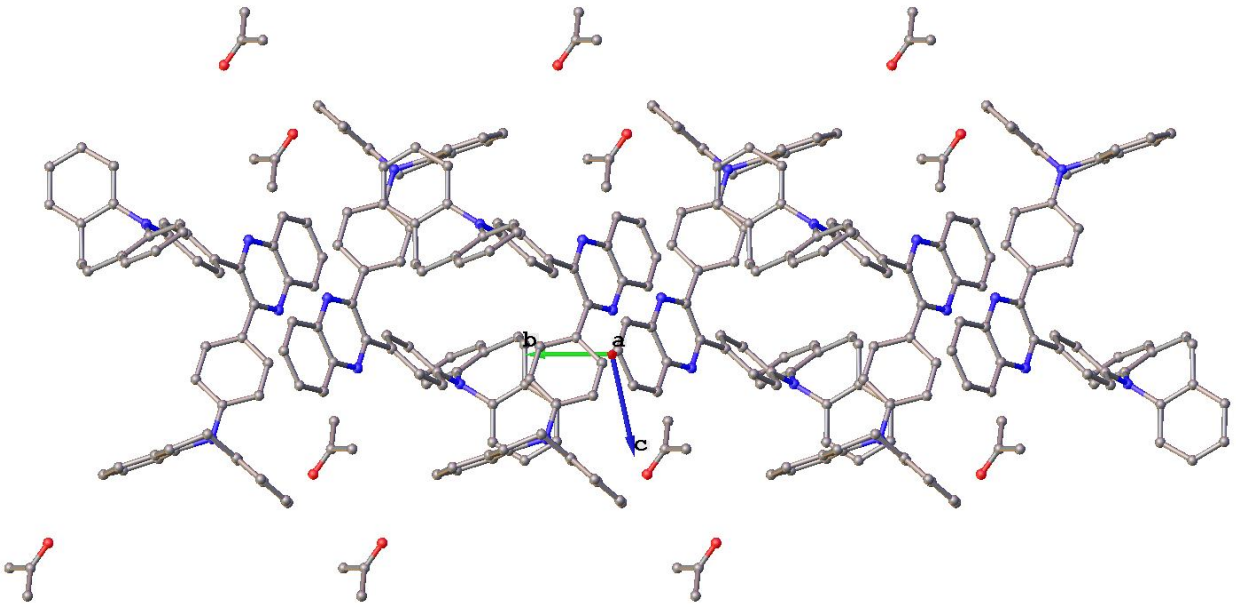

Figure S17. Packing in the crystal structure of compound IDBQx, viewed along the *a*-axis. Hydrogen atoms are removed for clarification

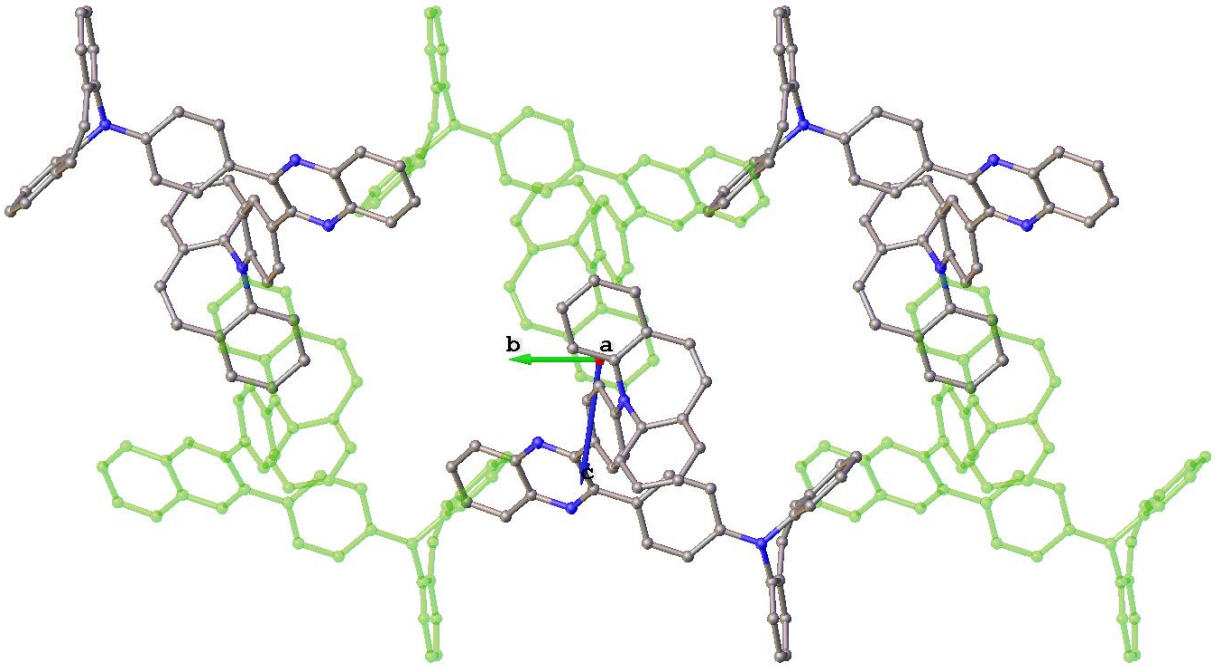

Figure S18. Packing in the crystal structure of compound ISBQx, viewed along the *a*-axis. Molecules have demonstrated with two colors for clarification

References:

1- C. A. Obafemi, W. Pfleiderer, *Helv. Chim. Acta*, 1994, **77**, 1549–1556.
2- I. S. Park, S. Y. Lee, C. Adachi, T. Yasuda, *Adv. Funct. Mater.*, 2016, **26**, 1813–1821.
3- K. Smith, D. M. James, A. G. Mistry, M. R. Bye, D. J. Faulkner, *Tetrahedron*, 1992, **48**, 4, 7479-7488.
4- O. V. Dolomanov, L. J. Bourhis, R. J. Gildea, J. A. K. Howard and H. Puschmann . *J. Appl. Cryst*., 2009, **42**, 339-341.
5- Sheldrick, G. M. *Acta Cryst.*, 2008, **64**, 112–122.

^{1}H and ^{13}C NMR of 2,8-dibromo-10,11-dihydro-5*H*-dibenzo[*b*,*f*]azepine:

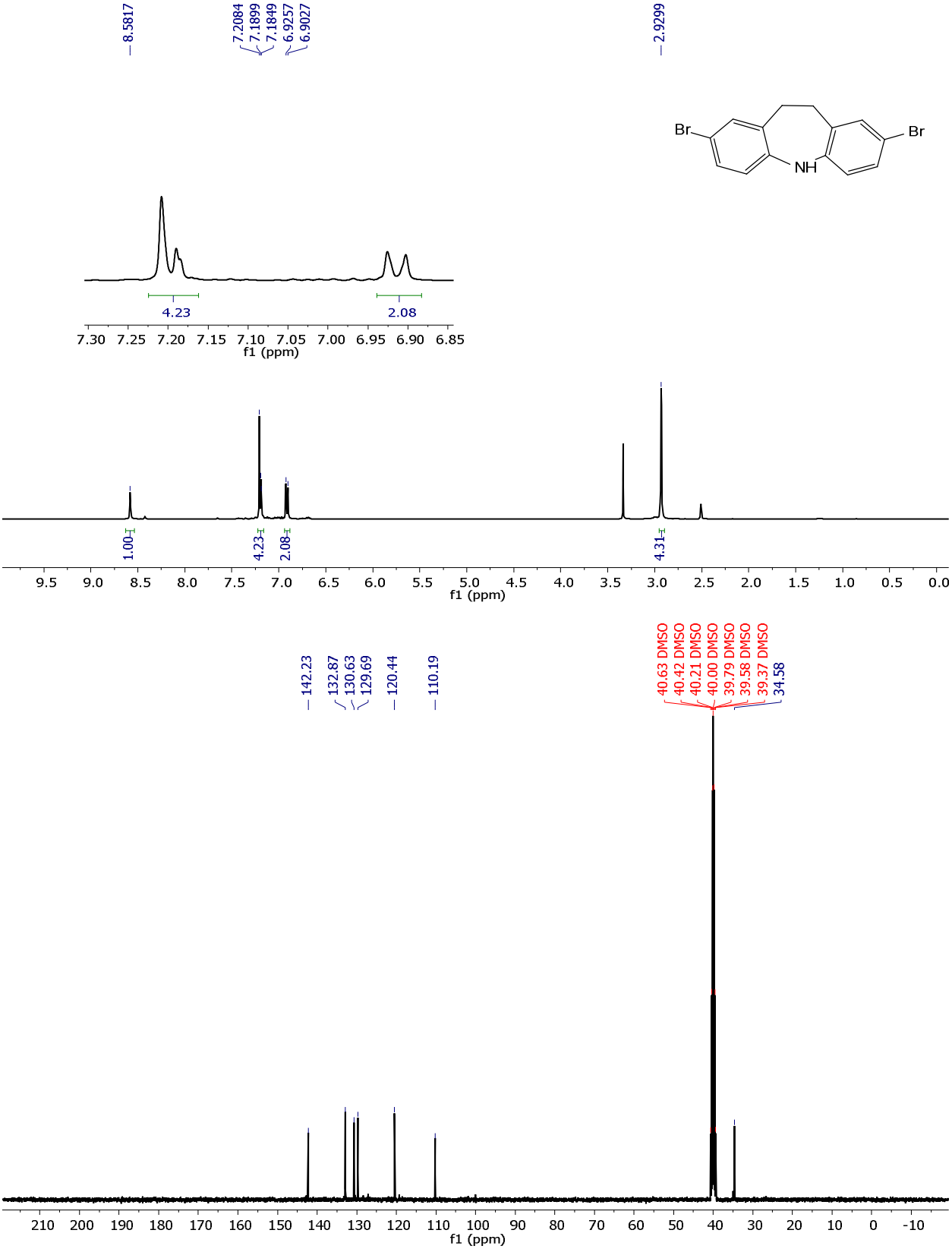

^{1}H and ^{13}C NMR of 2,8-dimethoxy-10,11-dihydro-5*H*-dibenzo[*b*,*f*]azepine:

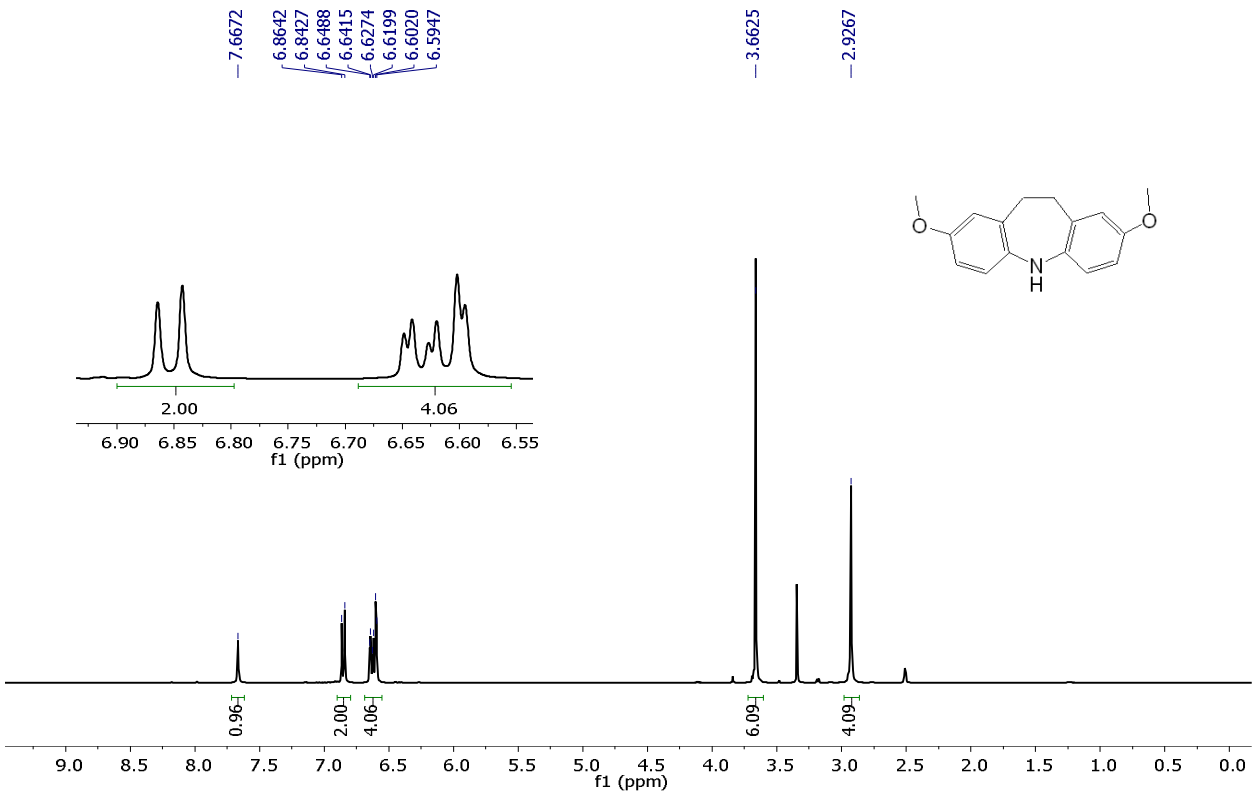

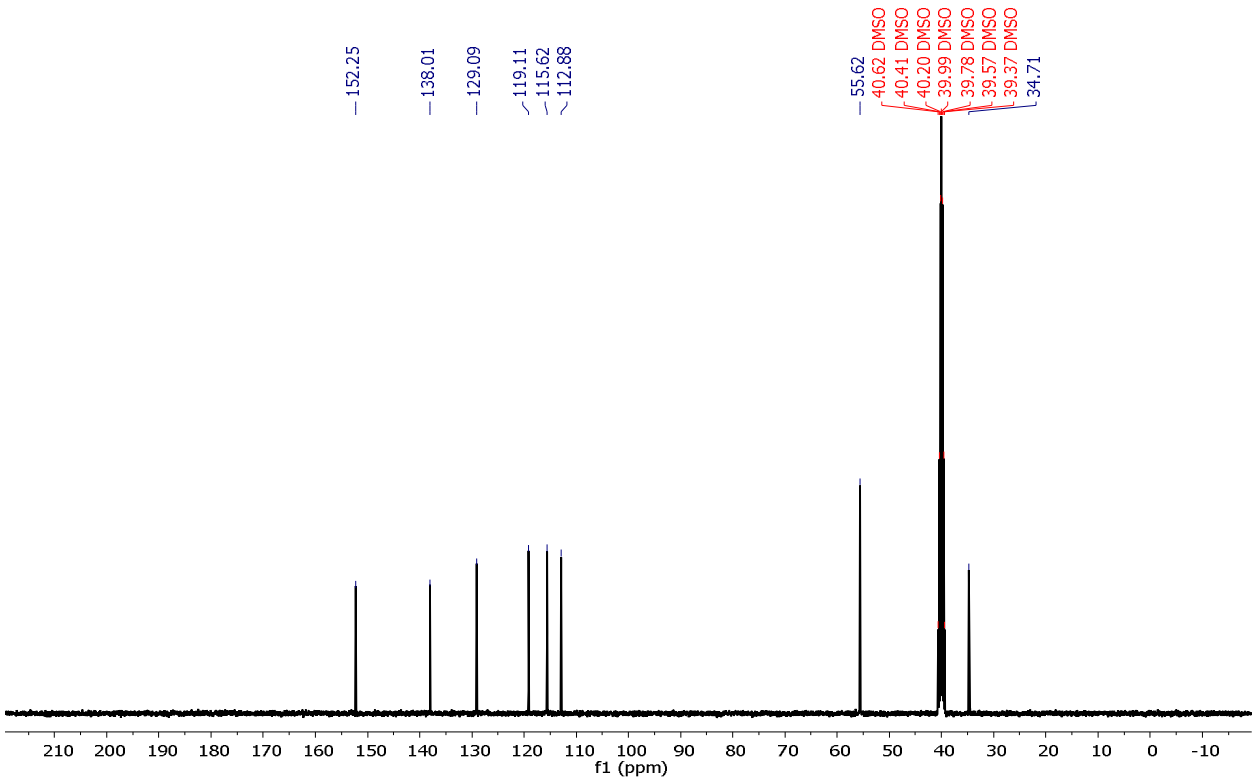

^{1}H and ^{13}C NMR of 2,3-bis(4-(10,11-dihydro-5*H*-dibenzo[*b*,*f*]azepin-5-yl)phenyl)quinoxaline (IDBQx):

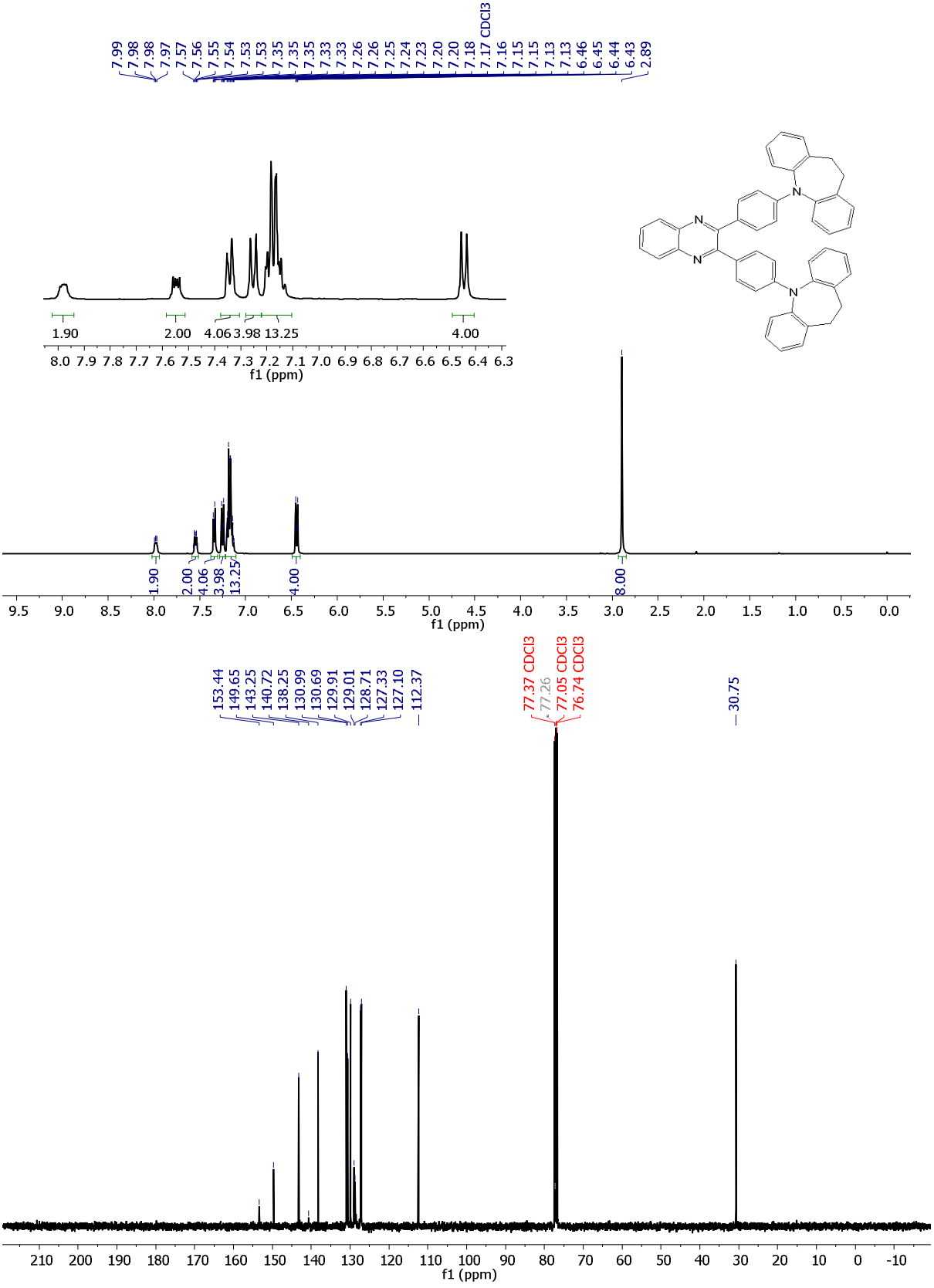

^{1}H and ^{13}C NMR of 2,3-bis(4-(5*H*-dibenzo[*b*,*f*]azepin-5-yl)phenyl)quinoxaline (ISBQx):

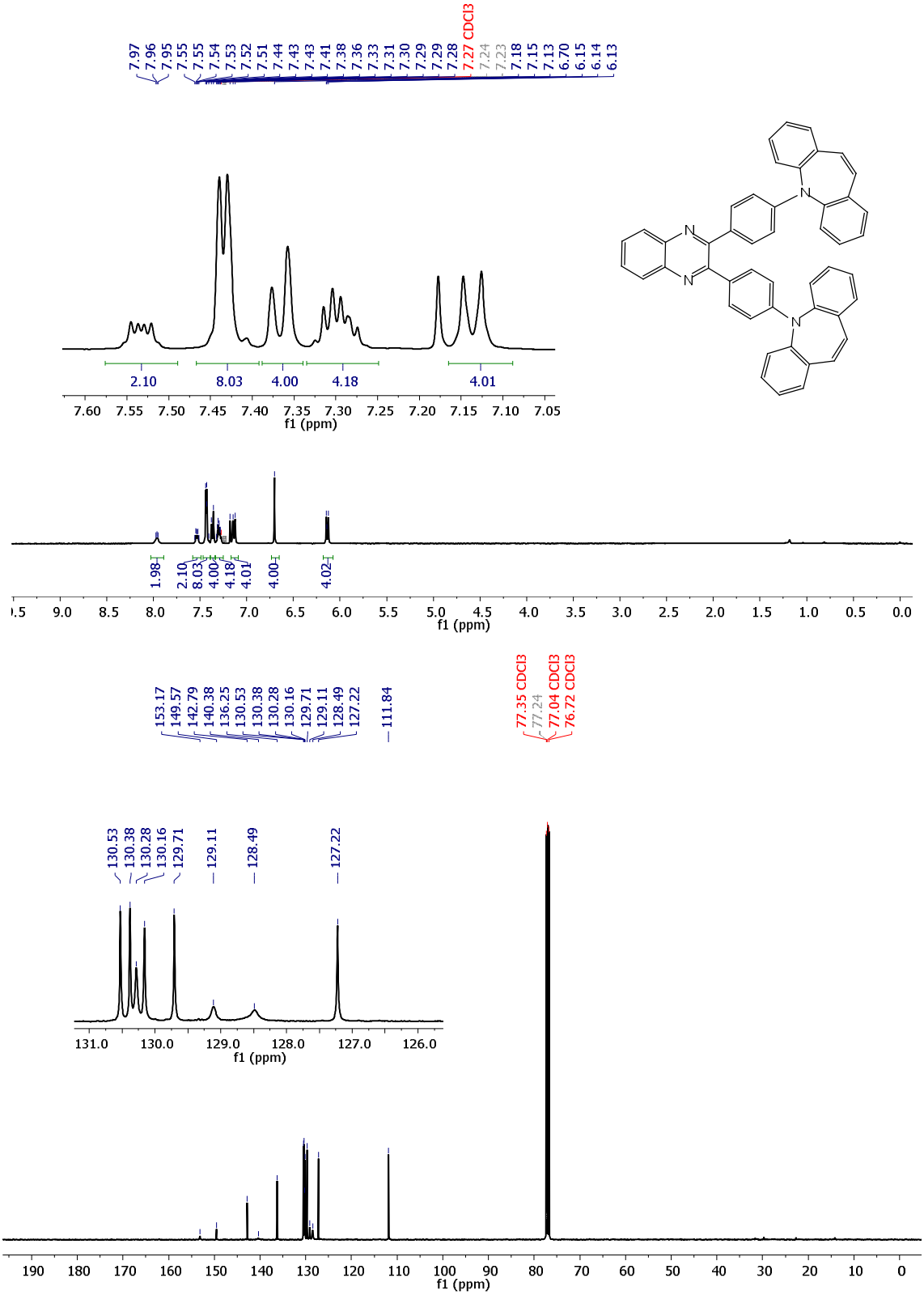

^{1}H and ^{13}C NMR of 2,3-bis(10,11-dihydro-5*H*-dibenzo[*b*,*f*]azepin-5-yl)quinoxaline (AzQx):

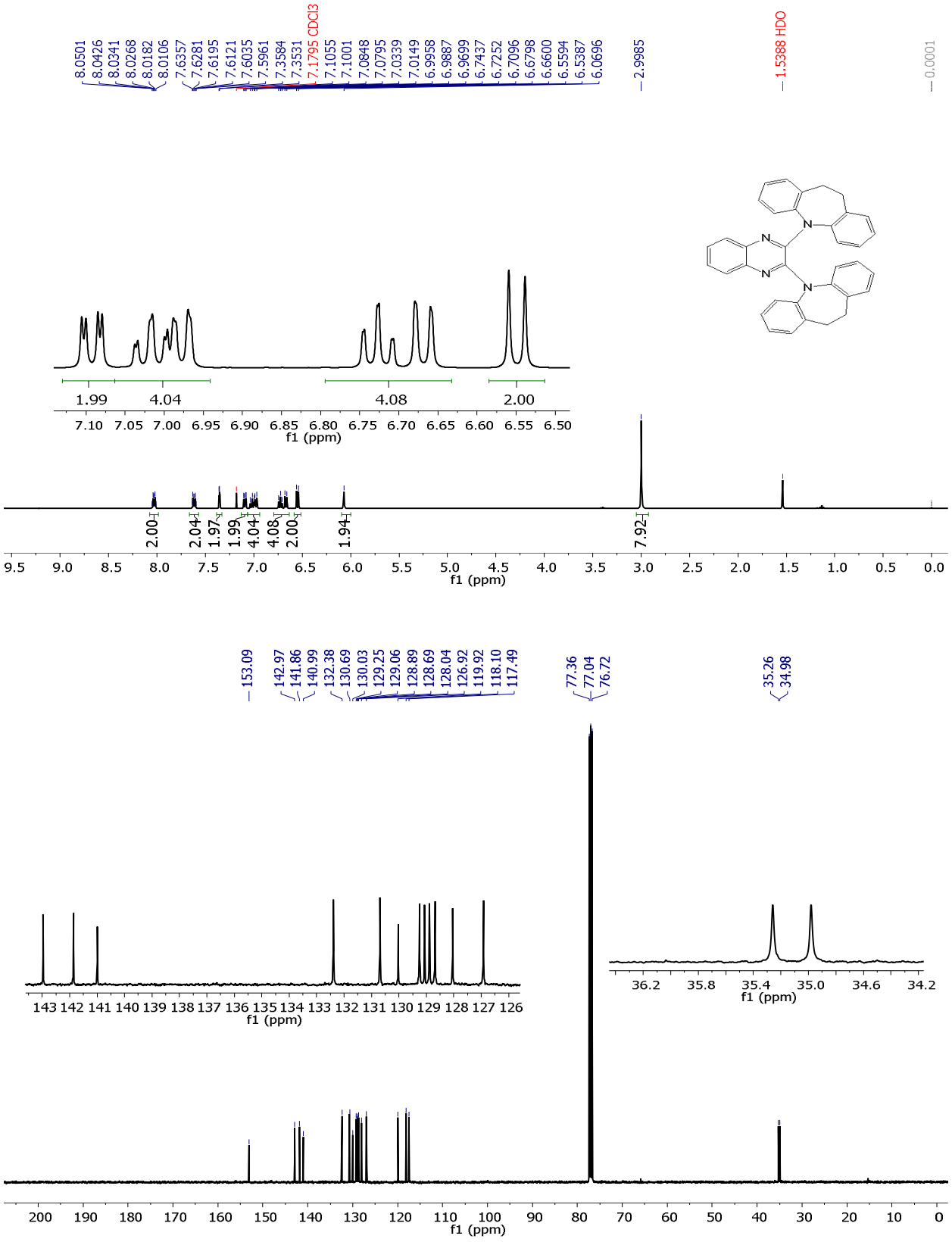

^{1}H and ^{13}C NMR of 2,3-bis(4-(2,8-dimethoxy-10,11-dihydro-5*H*-dibenzo[*b*,*f*]azepin-5-yl)phenyl)quinoxaline (OIDBQx):

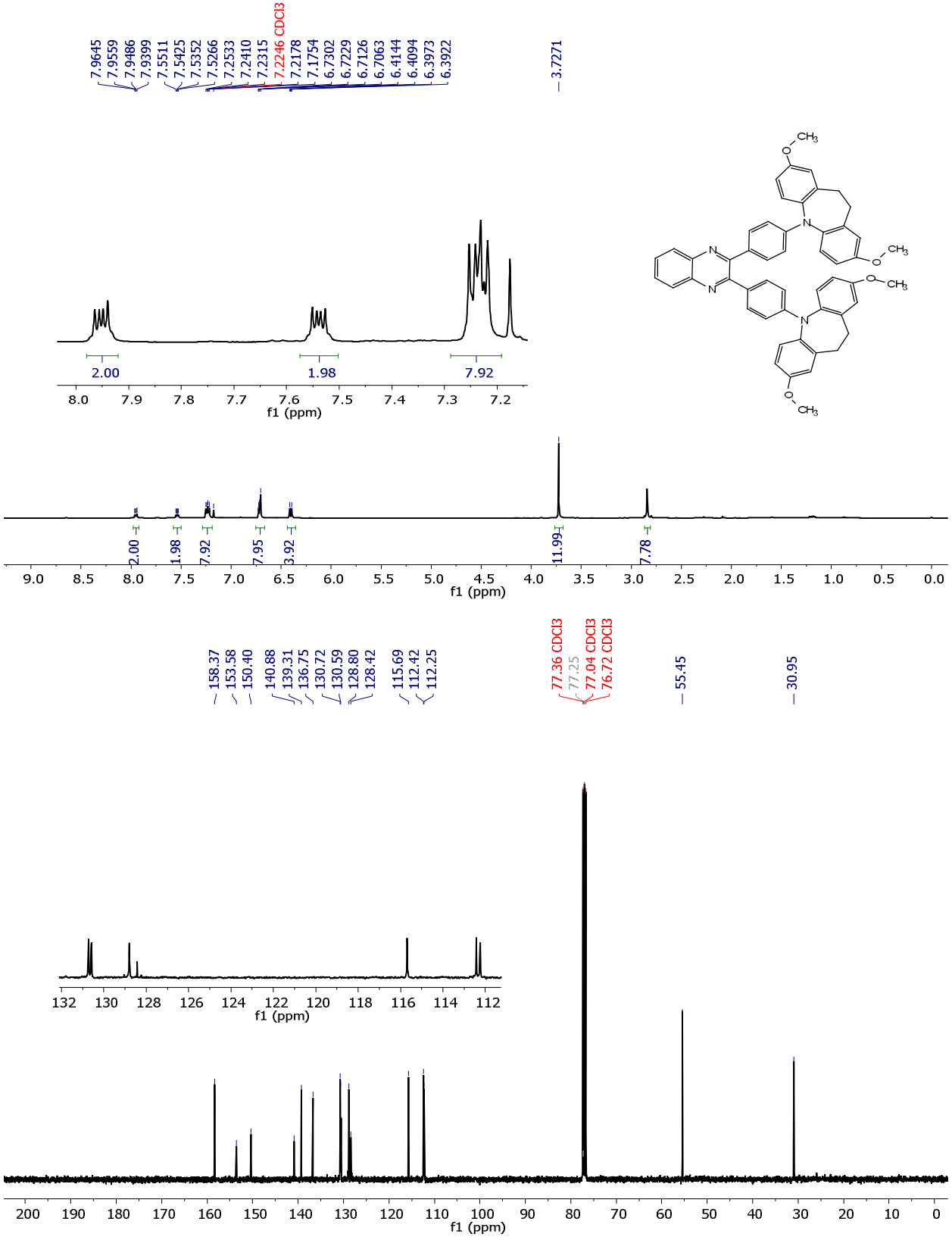

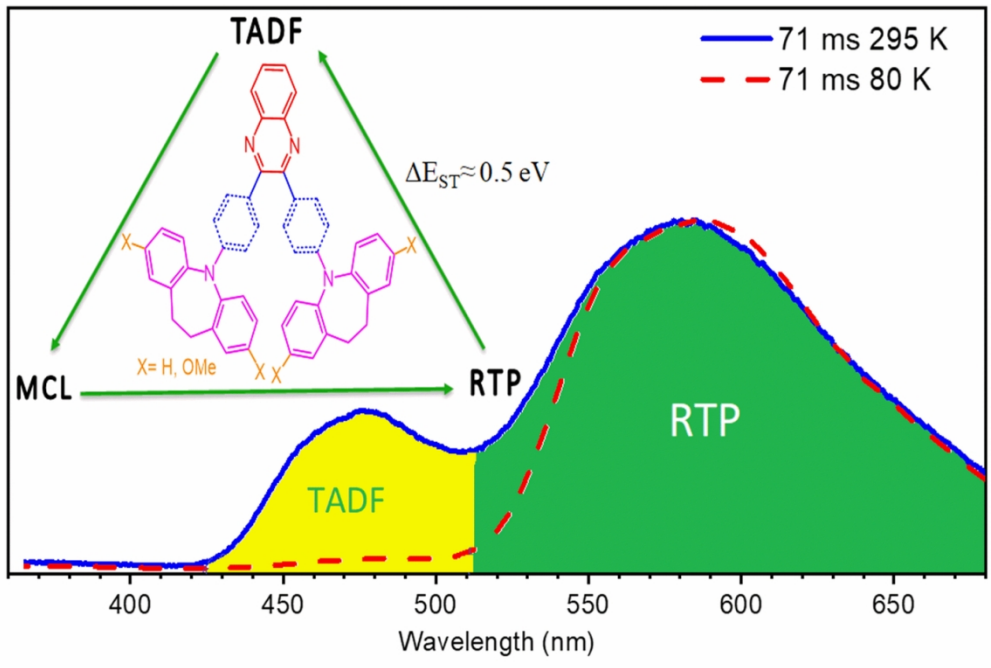

59x39mm (600 x 600 DPI)